Virus Entry is a Major Determinant of HCMV Latency in Monocytes

Yaarit Kitsberg, Aharon Nachshon, Tamar Arazi, Tal Fisher, Alexander Wainstein, Yaara Finkel,

Noam Stern-Ginossar*, Michal Schwartz*

Department of Molecular Genetics, Weizmann Institute of Science, Rehovot, Israel.

* To whom correspondence should be addressed: noam.stern-ginossar@weizmann.ac.il or michalsc@weizmann.ac.il

Abstract

Human Cytomegalovirus (HCMV) infection can result in either productive or latent infection, the latter being the basis for the virus life-long persistence. Intriguingly, monocytes, which support latent infection, become permissive to productive infection upon differentiation to macrophages. However, the molecular factors explaining these differentiation-driven differences are not fully understood and have been so far attributed to chromatin-mediated repression of the viral genome. Here, by using metabolic labeling of newly synthesized RNA early in monocyte and macrophage infection, we discover a major early block in viral gene expression, and viral transcripts are barely detected in infected monocytes. By unbiasedly analyzing the changes between monocytes and their differentiated counterparts, we reveal that the levels of several cell surface proteins involved in HCMV entry are upregulated upon monocyte to macrophage differentiation, and correspondingly we uncover HCMV entry into monocytes compared to macrophages is extremely inefficient. Remarkably, ectopic expression of a canonical HCMV entry receptor in monocytes facilitates productive infection of these cells, demonstrating that given efficient viral entry, monocytes, like macrophages, have the capacity to support productive infection. Among the cell surface proteins that are upregulated upon monocyte differentiation are several integrins, which we show play an important role in HCMV entry into macrophages, partially explaining the differences in viral entry. Overall, our findings reveal that a previously unrecognized major barrier for productive infection in monocytes is entry, adding a critical layer to the paradigm of HCMV latency.

Introduction

Human Cytomegalovirus (HCMV) is a human beta-herpesvirus infecting the majority of the population worldwide. Like other herpesviruses, HCMV persists through the lifetime of its host by establishing latency. Cells of the hematopoietic system were identified as key sites for HCMV latency. CD34+ hematopoietic stem cells (HSCs) and early progenitors of the myeloid system in the bone marrow as well as blood monocytes are the main cells in which HCMV latency has been characterized [1–3]. However, since CD14+ monocytes are short-lived, it has been proposed that the long-term latent reservoir resides in bone marrow HSCs [4]. In contrast, terminally differentiated myeloid cells such as macrophages and dendritic cells are considered permissive for productive HCMV infection, and differentiation to these cell types can lead to viral reactivation [5–8]. Since there is no suitable animal model for studying HCMV latency, much of the knowledge was gained from research performed in these cell culture models.

We previously showed that when macrophages are infected, the main factor that dictates productive infection is the initial levels of viral gene expression and specifically the expression of HCMV immediate early genes, IE1 and IE2 [9]. The accepted underlying assumption is that chromatin-dependent repression of the viral genome, and specifically of immediate early genes, is the basis for latent infection in monocytes and HSCs [10], and that differentiation leads to distinct chromatin deposition that enables viral gene expression [11,12]. However, the molecular roots for the differences in repression upon differentiation are not fully understood.

Here, using metabolic labeling of newly synthesized mRNA, we reveal that unlike in macrophages, early viral gene expression in undifferentiated monocytic cells is almost undetectable. By systematically comparing monocytes and their differentiated counterparts, we show that much of this variation is due to major differences in viral entry and that in monocytes, viral genomes rarely reach the nucleus. Remarkably, ectopic expression of the HCMV entry receptor PDGFRα in monocytes, enabled productive infection. This demonstrates that given efficient viral entry, monocytes have the capacity to support productive infection. We further reveal that several integrins that were previously associated with HCMV entry [13,14] are upregulated upon differentiation and play a critical role in macrophage infection. Overall, we uncovered that inefficient entry is a major factor that drives latent infection in monocytes and that integrins may play a central role in the differentiation-dependent susceptibility to productive infection in macrophages.

Results

Viral gene expression is undetectable at early stages of infection in monocytes

Monocytes are known to be latently infected with HCMV and do not support productive infection. However, following differentiation they become permissive to productive infection [5,6]. Indeed, we could recapitulate these differentiation-based differences in HCMV infection in primary blood monocytes as well as in the monocytic cell lines THP1 and Kasumi-3, which are commonly used as cell models to study HCMV latency. We infected these cell types with an HCMV TB40-E strain containing a GFP reporter (HCMV-GFP), which allows easy quantification of productively infected cells [15]. In the monocytic cells, GFP expression remained low (Fig. 1a) and correspondingly, no infectious progeny production was detected at 10 days post-infection (d.p.i) (Fig. 1b). In contrast, differentiation of the same cells to monocyte-derived macrophages prior to infection, resulted in a distinct population of cells that expressed high levels of GFP at 3 d.p.i, indicating productive infection (Fig. 1a) and indeed these cells produced infectious progeny (Fig. 1b). We recently showed that initial levels of viral gene expression are a major factor in dictating productive infection in macrophages [9]. Since our work and others have also shown that early in monocyte infection, newly transcribed RNA is masked by relatively high levels of virion-associated input RNA [16,17], we sought to directly measure early transcription of viral genes. We applied thiol (SH)-linked alkylation for metabolic sequencing of RNA (SLAM-seq)[18]. SLAM-seq facilitates the measurement of newly transcribed RNA based on 4-thiouridine (4sU) incorporation into synthesized RNA. After RNA is extracted, 4sU is converted to a cytosine analog using iodoacetamide, and these U to C conversions are identified and quantified by RNA sequencing. We applied SLAM-seq to both primary and THP1 monocytes and macrophages, starting labeling at 3 hours post-infection (h.p.i) for two and three hours (cells were harvested at 5 and 6 h.p.i). We obtained all characteristics of high-quality SLAM-seq libraries in both primary and THP1-derived cells; >5389 quantified genes and high U to C conversion rate (Fig. S1a). The levels of newly synthesized cellular transcripts were comparable between infected primary monocytes and macrophages, as well as between infected THP1 monocytes and THP1 macrophages in both two and three hours of labeling, indicating there are no major biases in our labeling (Fig. S1b). Remarkably, newly synthesized viral transcripts were almost undetectable in monocytes regardless of the labeling time, while in macrophages new viral transcripts were clearly detected after two hours of labeling and their relative fraction further increased at 3 hours of labeling (Fig. 1c). The newly synthesized viral transcripts were predominantly immediate early genes (UL122 and UL123), reflecting the initiation of a productive infection cycle (Fig. S1c). These results demonstrate that at early stages of infection in monocytes (both primary and THP1), viral genes are hardly transcribed, while in macrophages they are efficiently expressed.

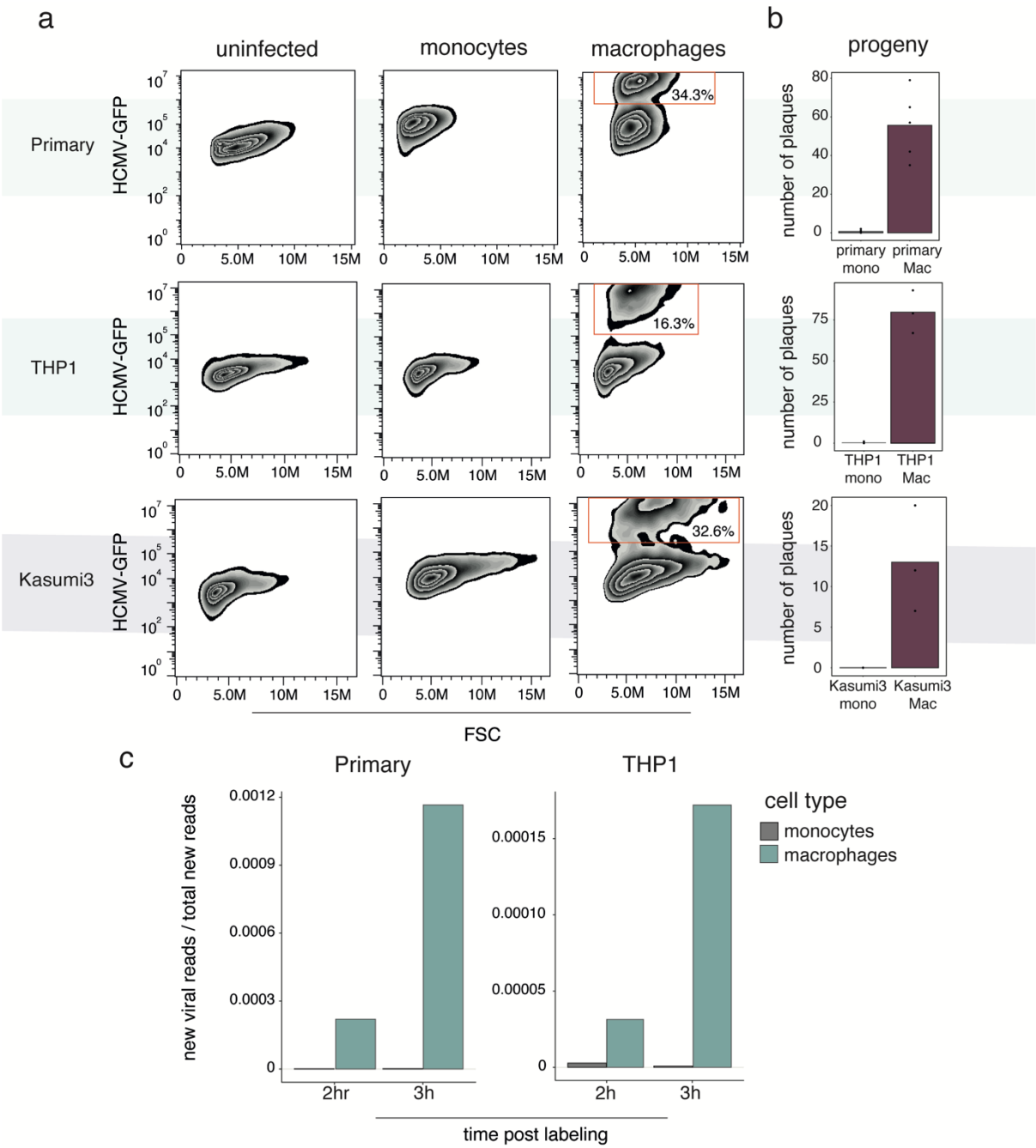

Fig. 1. HCMV infection and viral gene expression in monocytes and macrophages. (a). Flow cytometry analysis of primary, THP1 and Kasumi-3 monocytes and their differentiated counterparts infected with HCMV–GFP. Analysis was performed at 3 days post-infection (d.p.i). The red gate marks the productive, GFP-bright cell population. FSC, forward scatter; M, million. (b). Measurements of infectious virus in supernatants collected from infected monocytes and macrophages at 10 d.p.i. Mono, monocytes; Mac, macrophages. (c). Proportion of new viral reads out of the total new reads detected by SLAM-seq in infected primary and THP1 monocytes and macrophages. Infected cells were labeled with 4sU at 3 h.p.i. and harvested for SLAM-seq after 2 hours (left bars) or 3 hours (adjacent right bars) of labeling.

Cell surface proteins are upregulated upon monocyte differentiation to macrophages

The complete absence of newly synthesized viral transcripts in infected monocytes, compared to macrophages at such early stages in infection, indicates a fundamental difference in HCMV's ability to initiate gene expression in these two cell types. In order to unbiasedly search for candidate factors that may explain these dramatic differences, we performed RNA-seq on primary monocytes, THP1 monocytes and Kasumi-3 myeloid progenitor cells, as well as on macrophages derived from the same cells. Thousands of genes were differentially expressed upon differentiation (Table S1). Pathway enrichment analysis in each of the cell types (primary monocytes, THP1 and Kasumi-3 cells) revealed that common pathways change upon differentiation of THP1 and Kasumi-3 cells, while different pathways change upon differentiation of primary monocytes (Fig. 2a). In primary monocytes, the most significantly differential pathways were related to inflammation and innate immunity and mainly decreased upon differentiation, with interferon response pathways being the most significantly reduced (Fig. 2a). This is in line with our previous work showing that intrinsic expression of interferon stimulated genes (ISGs) is decreased upon differentiation, and that this reduction contributes to the increased susceptibility of macrophages compared to monocytes [9]. In THP1 and Kasumi-3, which are tumor-derived cell lines, the most significant changes were decrease in pathways related to cell proliferation, such as E2F targets, Myc targets and G2/M checkpoint (Fig. 2a). A significant reduction in these cells' proliferation capacity upon differentiation was previously described [19,20], and as we show below this reduction in proliferation likely plays a role in HCMV infection [21,22]. Significantly enriched pathways that were shared between all three cell types included a reduction in apical junction and myogenesis, both not intuitively related to myeloid differentiation processes or to early viral gene expression.

Parsimoniously, we expect the same mechanism to explain the difference in infection upon differentiation in all three cell types, thus in order to reveal molecular processes relevant for the different infection outcomes, we focused on common differentially expressed genes. Upon differentiation, 213 genes were commonly upregulated between primary, THP1 and Kasumi-3 cells, which is a significant overlap ($p < 10^{-5}$, Fig. S2a), and 42 genes were commonly downregulated in all three cell types ($p = 0.133$, Fig. S2a). Pathway enrichment analysis on the commonly upregulated genes yielded several pathways related to differentiation and maturation of immune cells and immune signaling (Fig. S2b). Since we revealed massive differences in initial viral gene expression, we next focused on processes that can potentially explain these differences. Although there is a major focus in the field on chromatin-related factors that regulate HCMV repression in monocytes [23,24], such factors, as a group, were not significantly enriched in the shared genes (Fig. S2c). Nevertheless, four chromatin-related factors were downregulated upon differentiation in the three cell types, including

CHD3, which is implicated in the repression of the HCMV genome through the recruitment of HDACs[25,26]. We therefore explored the potential involvement of histone deacetylation, which is reported to play a key role in the repression of HCMV, in blocking productive infection in monocytes and macrophages. We tested the ability of the potent HDAC inhibitor, TrichostatinA (TSA), which is known to induce expression of IE genes in THP1 cells [27], to induce productive infection in monocytes. While TSA treatment indeed led to an increase in the percentage of productively infected monocytes, a comparable effect was also observed in macrophages. Furthermore, the TSA effect was minor compared to the effect of differentiation, suggesting additional factors contribute to the differences between monocytes and macrophages (Fig. 2b, Fig. S2d).

Intriguingly, we noticed that as a group, cell surface proteins were significantly upregulated upon differentiation (p = 0.042, Fig. 2c), indicating that monocyte-to-macrophage differentiation leads to notable changes in cell surface composition. Since changes in cell surface proteins can affect viral entry, which in turn can lead to drastic differences in viral gene expression, we next examined if surface proteins that were previously associated with HCMV entry (Table S2, compiled based on [28] and other studies referred in the table) are upregulated upon monocyte differentiation. We found that surface proteins associated with HCMV entry are enriched in the common upregulated genes (Fig. 2c, $p = 0.0062$). These upregulated genes include NRP2, which mediates HCMV entry into non-fibroblasts cells (through the viral pentamer entry complex)[29] as well as two integrins, ITGB1 and ITGB3, which were shown to play a role in HCMV entry [28] (Fig. 2c and table S2). These changes in the expression of cell surface proteins, and specifically those involved in HCMV entry, pointed to possible unexplored differences in viral entry between monocytes and macrophages.

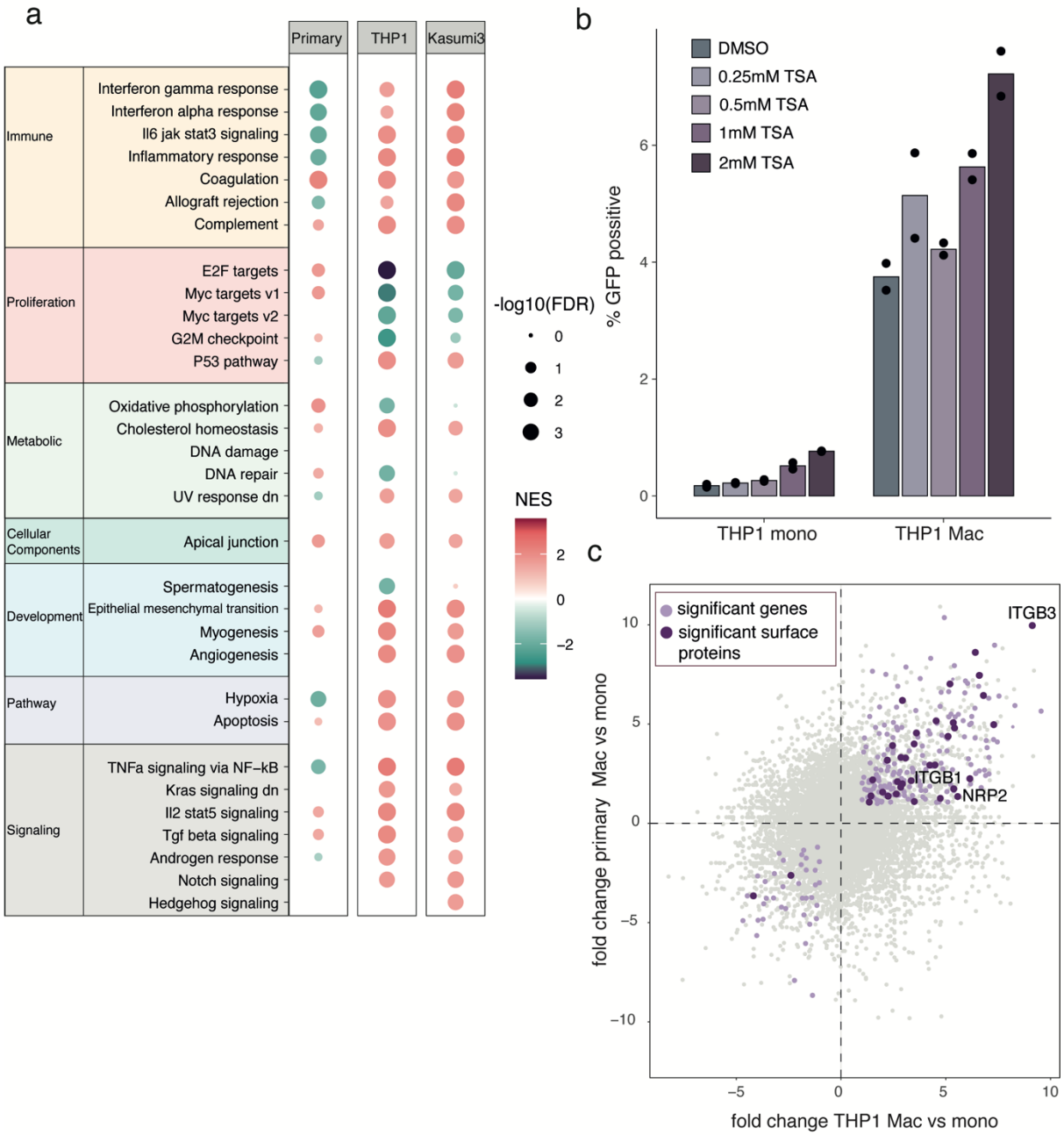

Fig. 2. Changes in cellular gene expression upon differentiation. (a). Summary of Hallmark pathway enrichment analysis of differentially expressed genes upon monocyte to macrophage differentiation in primary, THP1 and Kasumi-3 cells. FDR, false discovery rate; NES, normalized enrichment score. (b) THP1 monocytes and macrophages were treated with increasing concentrations of TSA. Cells were treated with TSA or DMSO control at 5 hours post infection (h.p.i). and analyzed at 3 d.p.i. by flow cytometry. (c) Scatterplot of the fold change (FC) from RNA-seq data between primary monocytes and macrophages, relative to the fold change of THP1 monocytes and macrophages. Light purple dots mark significantly changing genes (FDR < 0.05, FC > 1) in all three cell types. Dark purple dots mark single transmembrane genes that are significantly changing in all three cell types (P = 0.042). Names of significantly changing cell surface proteins in all three cell types involved in HCMV entry are shown (see Table S2).

Inefficient viral entry into monocytes is a major cause for the lack of viral gene expression

To explore if indeed disparities in viral entry may explain the drastic differences in viral gene expression, we quantified the number of viral genomes in the nuclei of infected primary and THP1 monocytes and macrophages by DNA FISH. We found that at 12 hours post-infection (h.p.i), almost none of the monocytes harbor viral genomes in their nuclei, while a considerable portion of macrophages harbor at least one viral genome (Fig. 3a and 3b). To further examine differences in entry efficiency, we utilized a virus in which the tegument protein UL32 is tagged with GFP (UL32-GFP, [30]), allowing fluorescent tracking of viral particles. In correspondence with our DNA-FISH measurements, we found considerably more viral particles within infected macrophages compared to infected monocytes (Fig. 3c and 3d).

To test if viral entry is indeed a critical barrier and overcoming it facilitates infection of monocytes, we ectopically expressed PDGFRα, the major entry receptor of HCMV into fibroblasts [31], which is not expressed in either monocytes or macrophages (Fig. S4a) in THP1 cells (THP1-PDGFRα, Fig. S4b). Remarkably, infection of THP1-PDGFRα with HCMV-GFP, resulted in a distinct population of GFP-bright cells at 3 d.p.i., indicating these cells are productively infected (Fig. 4a). Viral titers from infected THP1-PDGFRα were extremely low (possibly due to interference of the ectopically expressed PDGFRα with the release of viral progeny), however, these cells supported viral genome replication (Fig. 4b) and generated viral replication compartments (Fig. 4c), illustrating they support productive HCMV infection. Importantly, overexpression of PDGFRα did not result in differentiation of the cells, as the cells did not differ morphologically from the parental THP1 cells (Fig. S4c), or show any major changes in gene expression (Fig. S4d, Table S3), excluding the possibility of indirect effects of PDGFRα expression.

To substantiate that ectopic expression of PDGFRα in THP1 monocytes directly affects viral entry, we quantified viral genomes at 12 h.p.i. and found that in contrast to the parental THP1, In THP1-PDGFRα viral genomes reach the nucleus in a considerable portion of the cells (Fig. 4d). Furthermore, infected THP1-PDGFRα monocytes had significantly more viral particles in the cytoplasm than THP1 monocytes (Fig. 4e) and were actively transcribing viral genes at 5 h.p.i., as measured by SLAM-seq (Fig. 4f). Overall, these results demonstrate that inefficient entry of HCMV into monocytes is the major cause for the lack of viral gene expression and that efficient entry of viral genomes can facilitate productive replication even in monocytes.

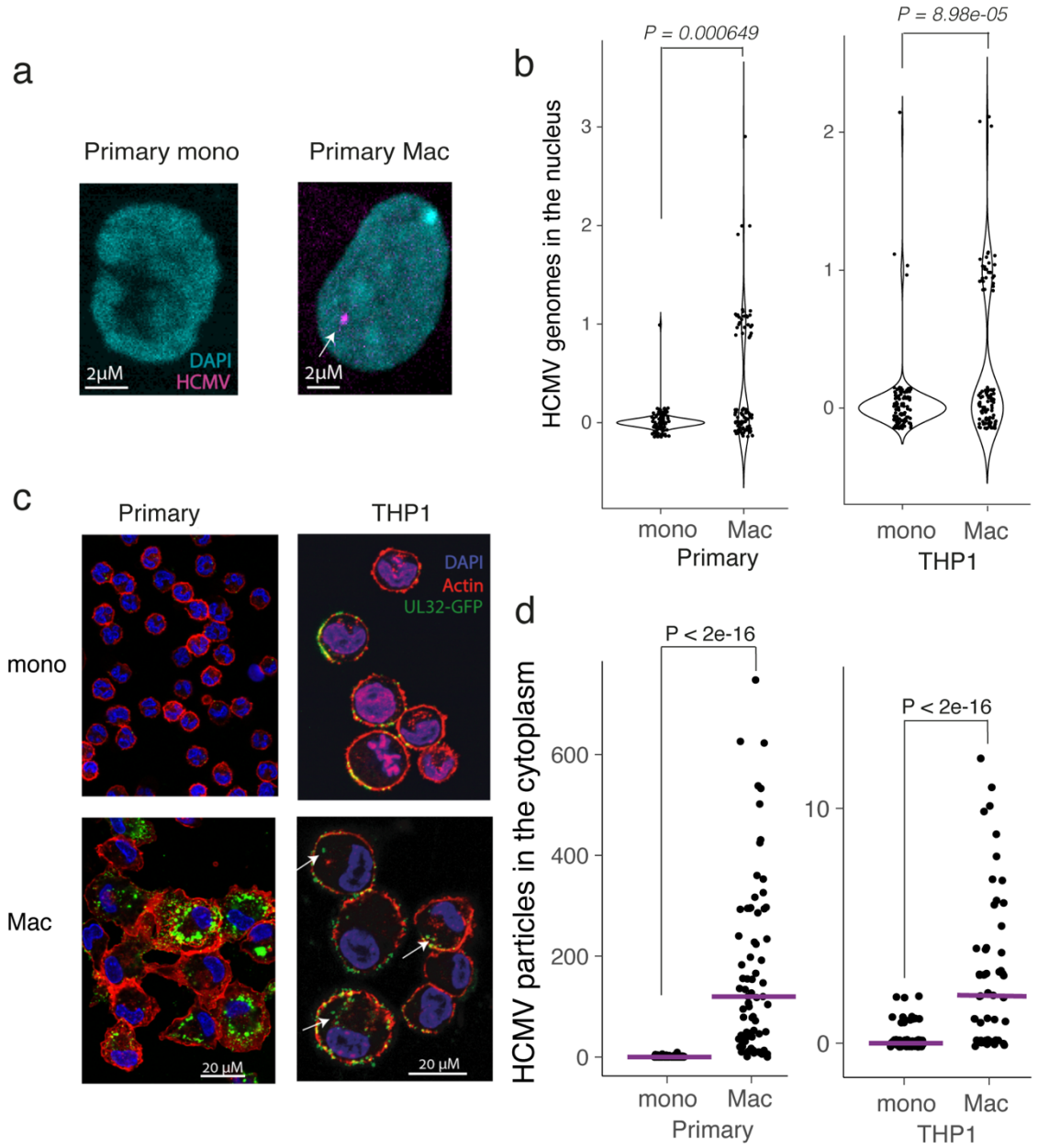

Fig. 3. HCMV is barely detected in the nucleus and cytoplasm of infected monocytes compared to macrophages. (a). Imaging of infected primary monocyte and macrophage nuclei at 12 h.p.i. The HCMV genome was probed using DNA-FISH. (b). Quantification of viral genomes detected in the nuclei of infected primary or THP1 monocytes (n=87 and n=112, respectively) and macrophages (n=93 and n=109, respectively) by DNA-FISH at 12 h.p.i. The P-value was calculated using Poisson regression. (c). Imaging of HCMV particles (UL32-GFP) in infected primary and THP1 monocytes and macrophages at 1 h.p.i. Actin staining was used to visualize cell borders and DAPI for the nuclei. (d). Quantification of viral particles within the cytoplasm of infected primary and THP1 monocytes (n=115 and n=78, respectively) and macrophages (n=71 and n=53, respectively) at 1 h.p.i (presented in c). Viral particles were counted using FIJI image processing and statistics was performed using Poisson regression. Mono, monocytes; mac, macrophages.

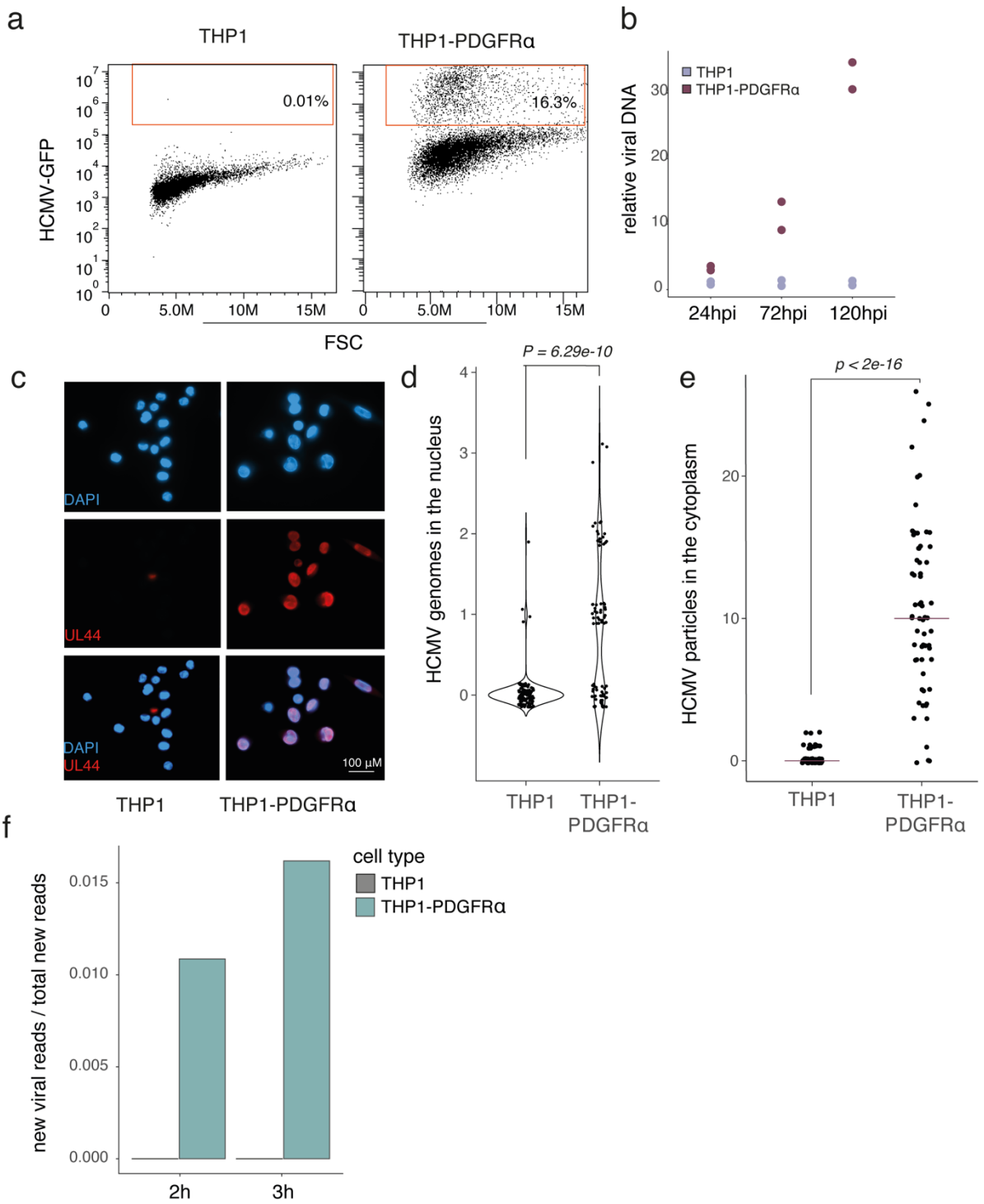

Fig. 4. Ectopic expression of* PDGFRα *in monocytes leads to productive infection. (a). Flow cytometry analysis of THP1 and THP1 overexpressing PDGFRα (THP1-PDGFRα) infected with HCMV–GFP at 3 d.p.i.. The red gate marks the productive, GFP-bright cell population. FSC, forward scatter. (b). Relative viral DNA levels in infected THP1 and THP1-PDGFRα at 24, 72 and 120 h.p.i. Viral DNA levels were measured by real-time PCR and were normalized to a cellular genomic target (c). THP1 and THP1-PDGFRα were infected with HCMV-GFP for four days. Cells were stained for UL44 (labeling the viral replication compartments) and analyzed by fluorescence microscopy (d). Quantification of the number of viral genomes in the nuclei of infected THP1 and THP1-PDGFRα monocytes at 12 h.p.i as detected by DNA-FISH (n=112 and n=84, respectively). P-value was calculated using

Poisson regression. (e). Quantification of the number of viral particles within the cytoplasm of infected THP1 and THP1-PDGFRα monocytes using HCMV-UL32-GFP at 1.h.pi. (n=78 and n=62, respectively). Viral particles were counted using FIJI image processing and statistics was performed using Poisson regression. (f). Proportion of new viral reads out of the total new reads detected by SLAM-seq in infected THP1 and THP1-PDGFRα monocytes. Infected cells were labeled with 4sU at 3 h.p.i. and harvested for SLAM-seq after two (left bars) or three (adjacent right bars) hours of labeling.

Integrins play a role in HCMV entry into macrophages

Our findings indicate that the different outcomes of HCMV infection in monocytes and macrophages are substantially driven by differences in viral entry. Moreover, several cell surface receptors implicated in HCMV infection are upregulated upon differentiation, three of them, NRP2, ITGB1 and ITGB3 are significantly upregulated in differentiation in all three monocytic cells tested. To test if their upregulation might explain the differences in viral entry, we examined whether any of these receptors are necessary for HCMV entry into macrophages.

We first focused on NRP2, which mediates HCMV entry into non-fibroblasts cells (through the viral pentamer entry complex)[29]. NRP2 transcript levels increased dramatically upon differentiation of monocytes to macrophages in the three cell types tested (Fig. 5a). Indeed, cell surface staining illustrated NRP2 is not expressed on the surface of monocytes and differentiation to macrophages was accompanied by low but detectable cell surface expression (Fig. 5b). To test if NRP2 is important for viral entry into macrophages, we used siRNA to knockdown NRP2 expression (Fig. S5a). Surprisingly, NRP2 knockdown did not affect the infection of THP1-derived macrophages, showing it likely does not mediate HCMV entry in these cells (Fig. 5c). To rule out lack of effect due to residual expression of NRP2 on the cell surface, we used CRISPR-Cas9 to generate THP1 cells in which NRP2 was knocked out (Fig. S5b). Infection of differentiated NRP2 knockout cells showed similar levels of infection compared to control cells (Fig. 5d), indicating NRP2 does not mediate HCMV entry into macrophages and its upregulation cannot explain the differences in viral entry. Importantly, since NRP2 mediates entry through the pentamer complex, and the genes encoding pentamer subunits are often mutated during viral propagation, we sequenced the virus (TB40 strain) we used for infection, and ruled out the possibility that accumulation of mutations in the genes encoding the pentamer explain lack of effect of NRP2 in these cells (see methods section).

Both ITGB3, which encodes integrin β3 and ITGB1, which encodes integrin β1, were significantly transcriptionally upregulated upon differentiation (Fig. 6a). These β subunits can dimerize with different α subunits to form canonical heterodimers, some of which were implicated in HCMV entry [14,32,33]. In agreement with our RNA-seq measurements, β3 surface expression was not detected in either primary or THP1 monocytes whereas in macrophages its expression was pronounced (Fig. 6b);

β1 was expressed on the surface of monocytes but its expression significantly increased in macrophages (Fig. 6c).

To dissect if these integrins play a role in HCMV entry into macrophages, we generated CRISPR knockouts of either ITGB3 or ITGB1 in THP1 cells (Fig. S6a). Knockout of ITGB1 did not affect HCMV productive infection in THP1-derived macrophages. However, in the absence of ITGB3, differentiated macrophages were much less susceptible to productive infection compared to control cells (Fig. 6d and 6e). We also tested the knockout effect of both ITGB3 and ITGB1 but observed no cumulative effect beyond the effect of ITGB3 knockout (Fig. 6d and 6e).

We validated these results by performing siRNA knockdown in THP1 macrophages (Fig. S6b), showing that knockdown of ITGB3 leads to a significant decrease in productive infection of macrophages (Fig. s6c and s6d). Furthermore, to directly test the effect on HCMV entry we infected control and ITGB3 knockout macrophages with UL32-GFP and tracked viral particles, revealing that in ITGB3 knockout macrophages viral entry was significantly inhibited (Fig. 6f and 6g). These results illustrate that the expression of several integrins significantly increases upon monocyte differentiation to macrophages and that the increase in ITGB3 expression plays a crucial role in the entry of HCMV and subsequently in promoting infection of macrophages.

We next explored whether ectopic expression of ITGB3 is sufficient to facilitate productive infection in monocytes. Since ITGB3 was shown to be involved in HCMV entry in a complex with ITGAV (integrin αV), which is also upregulated upon monocyte differentiation (table S2), we transduced THP1 cells with both ITGB3 and ITGAV under an inducible promoter. Following the induction of expression, we infected these cells with HCMV-GFP (Fig. S6e). Overexpression of ITGB3 and ITGAV in monocytes did not lead to an increase in productive infection compared to control cells (Fig. 6h and 6i). These results demonstrate that, although ITGB3 plays a role in HCMV entry into macrophages, its increased expression in macrophages alone is not the sole factor that facilitates the changes in viral entry and other proteins that are induced upon differentiation are likely required.

We further examined expression levels of NRP2, ITGB3 and ITGB1 in CD34+ HSCs which are also known to support HCMV latent infection, by analyzing published RNA-seq data from eight healthy patients [34]. NRP2 and ITGB3 are largely not expressed in these cells, while ITGB1 expression could be detected (Fig. 6j). This result is also supported by an additional study, showing rare expression of ITGB3 in CD34+ cells [35]. Therefore, the lack of surface proteins essential for HCMV entry is likely a major determinant for latent infection also in CD34+ HSCs.

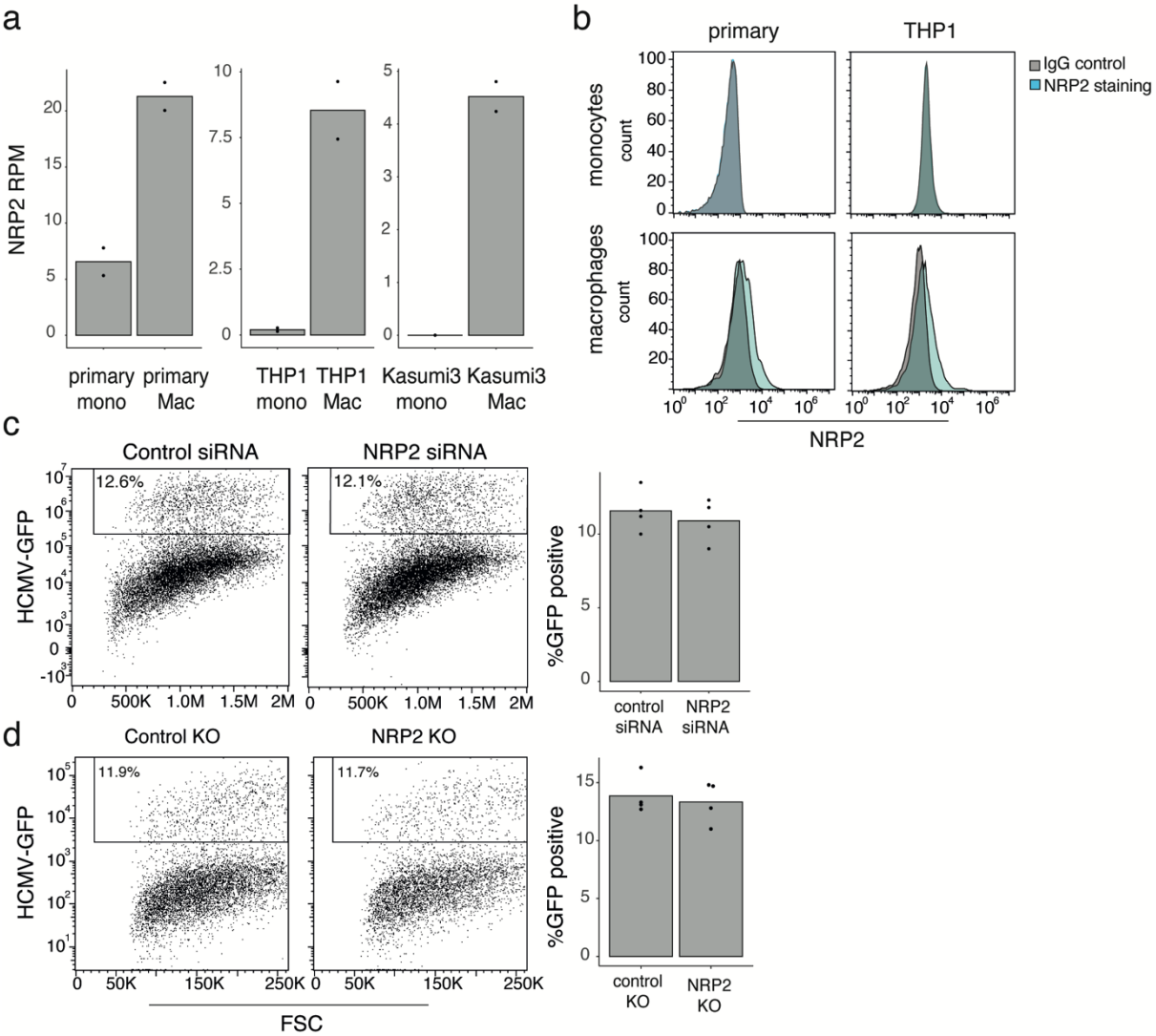

Fig. 5. NRP2 does not facilitate HCMV entry into macrophages. (a). NRP2 expression in primary, THP-1 and Kasumi-3 monocytes and macrophages as measured by RNA-seq. Mono, monocytes; mac, macrophages; RPM, reads per million. (b). Flow cytometry analysis of NRP2 versus IgG control Cell surface staining in primary and THP1 monocytes and macrophages. (c). Flow cytometry analysis of THP1 macrophages, transfected with NRP2 and control siRNA two days before infection with HCMV-GFP. Analysis performed at 3 d.p.i. Quantification of the replicates is presented on the right bar graph. (d). Flow cytometry analysis of infected THP1 macrophages with NRP2 or control CRISPR knockout using HCMV-GFP virus. Analysis performed at 3 d.p.i. Quantification of the replicates is presented on the right bar graph.

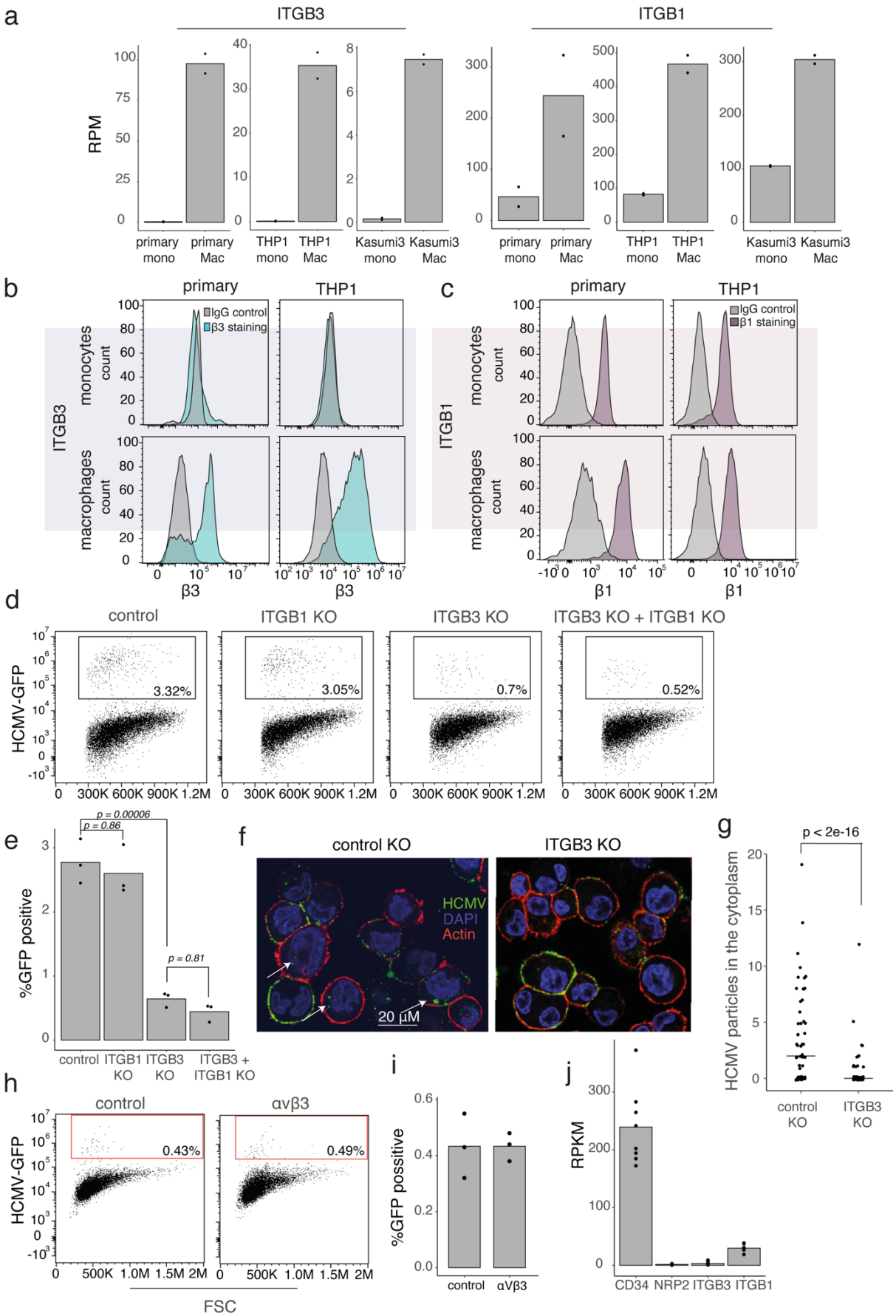
a
ITGB3
ITGB1
RPM
primary mono
primary Mac
THP1 mono
THP1 Mac
Kasumi3 mono
Kasumi3 Mac
b
primary
THP1
IgG control
β3 staining
monocytes
macrophages
count
ITGB3
β3
c
IgG control
β1 staining
ITGB1
β1
d
control
ITGB1 KO
ITGB3 KO
ITGB3 KO + ITGB1 KO
HCMV-GFP
3.32%
3.05%
0.7%
0.52%
e
p = 0.00006
p = 0.86
p = 0.81
%GFP positive
control
ITGB1 KO
ITGB3 KO
ITGB3 + ITGB1 KO
f
control KO
ITGB3 KO
HCMV
DAPI
Actin
20 µM
g
p < 2e-16
HCMV particles in the cytoplasm
control KO
ITGB3 KO
h
control
αvβ3
0.43%
0.49%
FSC
i
%GFP possitive
control
αVβ3
j
RPKM
CD34
NRP2
ITGB3
ITGB1

Fig. 6. HCMV entry into macrophages is mediated through ITGB3 (a). ITGB3 and ITGB1 expression in primary, THP1 and Kasumi-3 monocytes and macrophages as measured by RNA-seq. RPM, reads per million. (b-c). Flow cytometry analysis of integrin β1 (b) and integrin β3 (c) cell surface levels in primary and THP1 monocytes and macrophages. (d). Flow cytometry analysis of control, ITGB3, ITGB1 and ITGB3 + ITGB1 knockout (KO) in THP1 macrophages infected with HCMV–GFP. Cells were analyzed at 3 d.p.i. (e). Quantification of the replicates of Fig. 6d. (f-g). Representative Microscopy images (f) and quantification using FIJI analysis software (g) of THP1 macrophages with ITGB3 knockout (KO) versus control knockout (n=60 in the control and n=67 in the ITGB3 KO). Cells were infected with HCMV-UL32-GFP and imaged at 1.h.pi. Actin staining was used to visualize the cell's borders and DAPI for nuclei staining. (h). Flow cytometry analysis of infected THP1 monocytes overexpressing ITGB3 and ITGAV (αvβ3), compared to mCherry control. Overexpression was induced for 24 hours using doxycycline prior to infection. Cells were analyzed at 3 d.p.i. (i). Quantification of the replicates of Fig. 5i. (j). Expression levels of ITGB3, ITGB1 and NRP2 in CD34+ HSCs from RNA-seq of eight healthy patients [34]. RPKM, Reads Per Kilobase per Million mapped reads.

Genome-wide CRISPR screen reveals additional unexpected barriers for productive infection in monocytes

THP1-PDGFRα cells can be used to circumvent the entry barrier for infection in monocytes, enabling us to unbiasedly explore which additional factors affect monocyte infection, by conducting a genome-wide CRISPR knockout screen (Fig. 7a). THP1-PDGFRα were transduced with the GeCKO CRISPR/Cas9 knockout library, which targets 19,050 human genes with three guides per gene and one thousand non-targeting gRNA as controls [36], at low multiplicity of infection to ensure expression of a single gRNA in each transduced cell. We infected these cells with HCMV-GFP and at 2 d.p.i. sorted them to GFP-bright and GFP-dim populations, reflecting productive and non-productive infection, respectively. gRNAs were sequenced from both populations, showing a high correlation between replicates (Fig. S7a). By using MAGeCK analysis [37] we defined genes whose gRNAs are significantly enriched in the non-productive or the productive populations, representing factors enhancing or limiting productive infection, respectively (Fig. 7b). Reassuringly, one of the top enhancing factors was PDGFRα (which was overexpressed in all cells) illustrating our screen captured genes whose targeting affects HCMV infection in these monocytes. Remarkably, almost all (9 out of 11) of the factors enhancing productive infection with fold change greater than 2 are related to the biosynthesis of proteoglycans and more specifically, to the biosynthesis or modification of heparan sulfate proteoglycans (HSPGs), which are known to be required for HCMV entry [38], further emphasizing the critical role of viral entry efficiency in controlling infection outcome in monocytes. Intriguingly, analysis of the expression of genes related to heparan sulfate deposition revealed that many of the heparan sulfate related genes that enhance productive infection in our screen are also upregulated upon differentiation (Fig, S7b). These findings

suggest that heparan sulfate levels or composition might also differ upon monocyte differentiation and contribute to the differences we observed in viral entry between monocytes and macrophages.

None of the genes limiting productive infection were statistically significant (Fig. 7b) but gene set enrichment analysis of screen scores revealed significant enrichment in genes related to DNA repair and E2F targets (Fig. 7c). These results suggest that the proliferative capacity of THP1 cells also inhibits HCMV productive infection. To explore this possibility, we compared infection between THP1-PDGFRα cells under normal growth conditions and under serum starvation. Serum starvation resulted in a significant increase in cells in G0/G1 phase (Fig. S7c) and significantly more productively infected cells (Fig. 7d), indicating that the proliferative nature of THP1 monocytes inhibits HCMV infection. Given the significant reduction in cell proliferation following differentiation of THP1 and Kasumi-3 cells (Fig. 3b and [19]), it is likely that in these highly proliferative cells, the differentiation-associated reduction in proliferation also contributes to the differences in susceptibility to productive HCMV infection in monocytes compared to macrophages.

Beyond biosynthesis of proteoglycans, factors enhancing productive infection were significantly enriched in genes related to oxidative phosphorylation and glycolysis (Fig. 7c). Interestingly, many of the oxidative phosphorylation genes which enhance productive infection in the screen, were also significantly upregulated upon monocyte differentiation (Fig. 7e, $p = 4.5\text{x}10^{-13}$). This suggests that increased oxidative phosphorylation capacity may also contribute to increased permissiveness of macrophages compared to monocytes. We tested whether oxidative phosphorylation levels affect productive infection by utilizing ionophore Carbonyl cyanide m-chlorophenyl hydrazone (CCCP), which reduces the mitochondrial membrane potential and inhibits oxidative phosphorylation. Inhibition of oxidative phosphorylation using CCCP at concentrations that reduced oxidative phosphorylation (Fig. S7d) but did not affect cell viability (Fig S7e) resulted in a significant decrease in the amount of productively infected THP1-PDGFRα monocytes (Fig. 7f and S7f), thus validating the screen results. Moreover, also in primary monocyte-derived macrophages, CCCP treatment that did not affect cell viability (Fig S7e), reduced productive infection (Fig 7g and S7g). These results suggest that the differentiation-induced increase in the expression of oxidative-phosphorylation genes contributes to the increase in HCMV permissivity upon monocyte differentiation.

Taken together, our results suggest that inefficient entry of HCMV into monocytes constitutes a major barrier to productive infection and is therefore a crucial factor leading to latent infection in these cells. The screen we performed revealed additional cellular processes such as cell proliferation and oxidative phosphorylation that change upon differentiation and affect the ability to establish infection in monocytes, likely further contributing to the establishment of latency in undifferentiated monocytic cells.

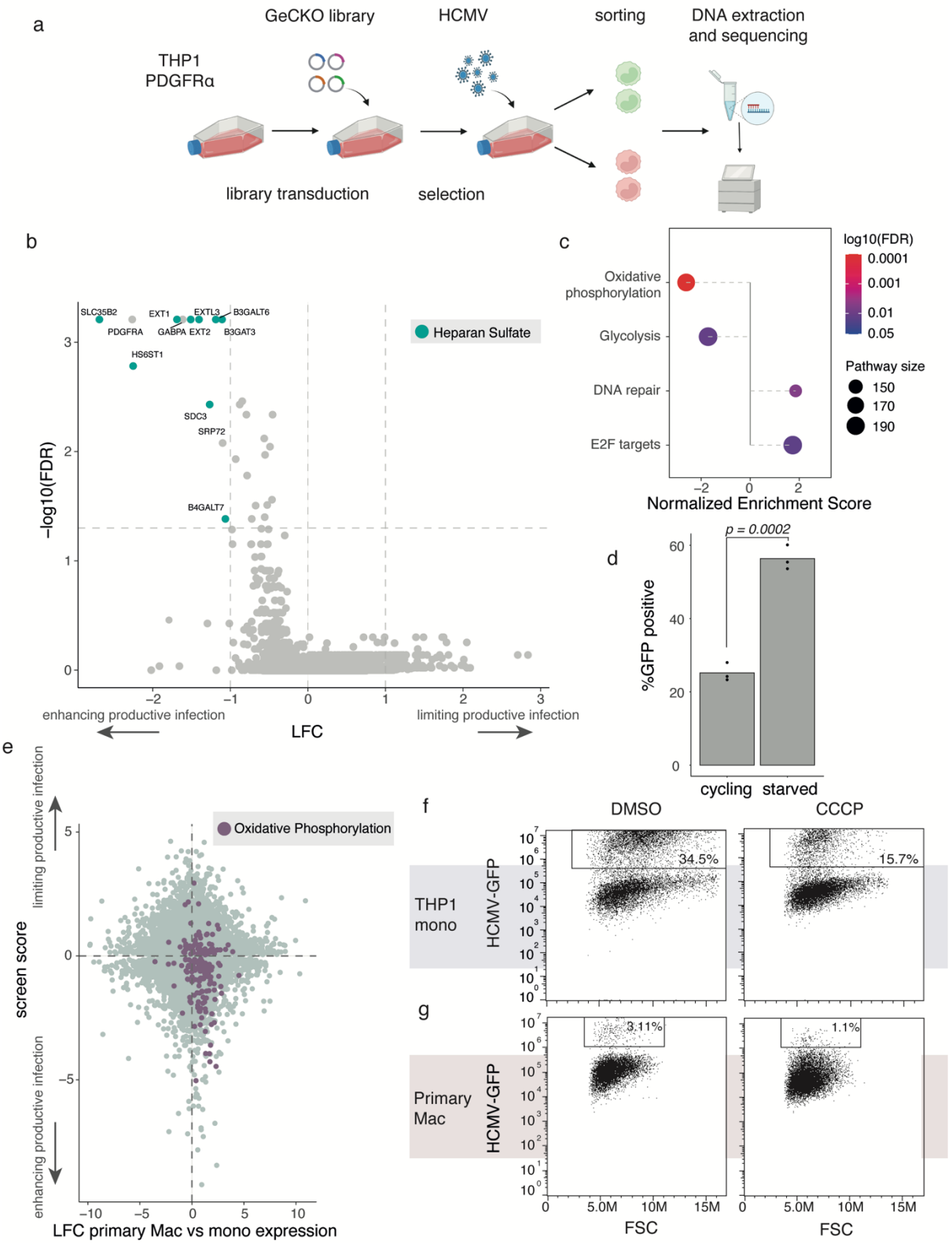

Fig. 7. Genome-wide CRISPR screen identifies entry mechanisms, oxidative phosphorylation and proliferation as critical factors for HCMV infection in monocytes. (a). Schematic overview of the genome-wide CRISPR screen on infected THP1-PDGFRα monocytes. Cells were transduced with the genome-wide GeCKO

library and selected using puromycin. After recovery from selection, cells were infected with HCMV-GFP and sorted to GFP-bright and GFP-dim populations at 2 d.p.i.. (b). Volcano plot showing changes in gRNAs levels in the GFP-bright population (right side, genes limiting productive infection) versus the dim population (left side, genes enhancing productive infection). For each gene, the FDR and the mean fold change was calculated using MaGECK. Horizontal dashed line represents an FDR threshold of 0.05 and vertical lines represent LFC > |1| and 0. FDR, false discovery rate; LFC, log fold change. (c). Summary of gene set enrichment analysis of differentially represented genes using Hallmark pathways. (d). Quantification of productive infection by flow cytometry analysis of HCMV–GFP infected cycling (20% FBS) and starved (0.5% FBS) THP1-PDGFRα monocytes. Analysis was performed at 3 d.p.i. (e) Scatter plot of MaGECK score of each gene against log fold change (LFC) of expression in primary monocytes versus macrophages. Oxidative phosphorylation-related genes are enriched in the bottom right quadrant ($p=4.5x10^{-13}$ as calculated by a proportion test). (f-g). Flow cytometry analysis of HCMV-GFP infection of CCCP drug-treated THP1-PDGFRα monocytes (f) or primary macrophages (g) compared to DMSO control. Cells were treated with CCCP for 1 hour before infection and analyzed at 3 d.p.i.

Discussion

HCMV infection of monocytes results in a latent infection in which the virus is largely repressed and does not replicate, while following differentiation of these cells, they become permissive to productive infection and produce progeny.

Previous studies have shown that latent infection is characterized by extremely low levels of viral transcripts [4,39]. Using metabolic labeling, we show that viral gene transcription is nearly absent in monocytes while substantial in macrophages, suggesting that viral gene expression is effectively inhibited in monocytes. Chromatin regulation has been implicated as a major factor for viral repression during latency [10,12]. Although some specific chromatin factors have been attributed to this repression [40–42], the differences between monocytes and their differentiated counterparts with regard to chromatin repression remain poorly defined. Our findings indicate that chromatin-based repression alone does not explain why monocytes fail to support a productive infection outcome. Chromatin repression can be relieved in both monocytes and macrophages using HDAC inhibitors, but productive infection in monocytes remains limited.

We found a striking disparity in the abundance of viral genomes within the nuclei of infected monocytes compared to macrophages at early time points, in line with previous studies of monocyte infection [43], and, notably, a significant difference in the quantity of viral capsids within these cells. This strongly suggests HCMV entry efficiency is a major unexplored barrier for productive infection in monocytes. Remarkably, ectopic expression of the HCMV entry receptor PDGFRα in monocytes facilitated productive infection, underscoring inefficient entry as the primary barrier in these cells. This

means that although monocytes are capable of supporting productive infection, they do not reach the required threshold of viral genomes due to entry limitations.

By performing unbiased transcriptome analyses, we interestingly found significant upregulation upon differentiation of several cell surface proteins which are linked to the entry of HCMV. In search of the relevant entry receptors, we first tackled NRP2 which mediates HCMV entry into non-fibroblast cells, through the viral pentamer complex. Although its expression increased during differentiation, our results indicate that it does not play a major role in viral entry into macrophages, at least with the TB40 strain. ITGB3 and ITGB1 were both shown to play a role in HCMV entry [14,32,44] and depletion of these integrins showed that ITGB3, which is not expressed in monocytes, is required for HCMV entry into macrophages. However, overexpression of ITGB3 with its canonical partner, ITGAV, was not sufficient to enable productive infection in monocytes, indicating the involvement of additional factors that are required for entry and absent in monocytes.

The notion that entry constitutes a major barrier for productive infection suggests that the number of particles that infect a cell plays a major role in the probability of establishing productive versus latent infection. This raises the possibility that the cell type and possibly different cell states also affect the potential of cells to become latently infected through effects on viral entry efficiency. For instance, infection at low multiplicity of infection, potentially in any cell type, can result in a subset of cells carrying an amount of genomes or particles which is too low to establish productive infection, possibly becoming repressed and maintaining latency. Furthermore, exposure to interferons may affect the efficiency of entry, thereby affecting the likelihood of cells to establish productive infection. Other factors that determine infection outcome, such as transcriptional repression, may be different between different cell types, and affect the threshold for the amount of viral particles that are required to establish productive infection.

Overcoming the entry barrier by PDGFRα ectopic expression allowed us to systematically screen for additional factors affecting the ability to establish productive infection in monocytes. We found that the proliferation level of monocytic cell lines affects the level of productive infection, in line with previous results[45]. We also show that oxidative phosphorylation genes are upregulated with differentiation and oxidative phosphorylation levels are important for establishing productive infection in monocytes and macrophages. Oxidative phosphorylation is known to be upregulated by HCMV and required for viral propagation [46–48], our results further show that the oxidative phosphorylation state at the time of infection affects its outcome.

Overall, we have revealed several processes that contribute to latency establishment in monocytes. Specifically, we uncover inefficient entry as the critical barrier for productive infection in monocytes. These results indicate that the quantity of viral particles entering a cell is a key determinant of the

virus's ability to initiate gene expression and ultimately dictates the outcome of infection. Thus, the propensity of a given cell type to support productive HCMV infection is governed by several interrelated factors: (1) the efficiency of viral entry, (2) the levels of antiviral mechanisms that repress viral gene expression, and (3) additional cellular processes that may enhance or inhibit infection, such as cell cycle stage or levels of oxidative phosphorylation. Our findings have far-reaching implications for understanding of how latency is established *in vivo* and which cell types can serve as latency reservoirs.

Material and Methods:

Ethics statement

All fresh peripheral blood samples were obtained after approval of protocols by the Weizmann Institutional Review Board (IRB application 92-1) and following informed consent from the donors. Blood donors were not compensated.

Cell culture and virus

Primary CD14+ monocytes were isolated from fresh venous blood, obtained from healthy donors, males and females, aged 25–45, using a Lymphoprep (Stemcell Technologies) density gradient followed by magnetic cell sorting with CD14+ magnetic beads (Miltenyi Biotec). Monocytes were cultured in X-Vivo15 media (Lonza) supplemented with 2.25 mM L-glutamine at 37 °C in 5% CO2, at a concentration of 1–2 million cells per ml in non-stick tubes to avoid differentiation.

Where indicated, primary monocytes were treated with 50 ng/ml PMA immediately following isolation and plating for 3 days. The treatment was performed in RPMI with 20% heat-inactivated fetal bovine serum (FBS), 2 mM L-glutamine and 100 units ml−1 penicillin and streptomycin (Beit-Haemek), and macrophages were grown in this media following treatment.

293T cells (ATCC CRL-3216) and Primary human foreskin fibroblasts (ATCC CRL-1634) were maintained in DMEM with 10% FBS, 2 mM L-glutamine and 100 units ml−1 penicillin and streptomycin (Beit-Haemek).

THP1 cells, purchased from ATCC (TIB-202), and Kasumi-3 cells, purchased from ATCC (CRL-2725), were grown in RPMI media with 20% heat-inactivated FBS, 2 mM L-glutamine and 100 units/ml penicillin and streptomycin (Beit-Haemek). Differentiation of THP1 and Kasumi-3 cells was done by adding 50 ng/ml PMA for 3 days.

Infection and growth following infection were done in media containing 20% or 0.5% FBS for cycling and starved experiments, respectively.

The TB40E strain of HCMV, containing an SV40–GFP reporter, was described previously [15]. The virus was propagated by adenofection of infectious bacterial artificial chromosome DNA into fibroblasts as described previously (Elbasani et al., 2014). The complete genome sequence of the virus was determined by Illumina sequencing using NEBNext® DNA Library Prep Kit.
For microscopy imaging, a previously reported TB40E strain containing GFP fused to a tegument protein (UL32-GFP) was used [30].

Infection procedures

Infection was performed by spinfection at multiplicity of infection (MOI) = 5 at 800g for 1 h, washing and supplementing with fresh media. Notably, because this MOI is based on quantification of infectious particles in fibroblasts it is effectively lower in monocytic cells.
For progeny assay, at 10 d.p.i. The supernatant was cleared from cell debris by centrifugation and transferred to 7,500 fibroblasts per well in 96-well plates, and infected cells were counted 3 days later.

Flow cytometry and sorting

Cells were analyzed on a BD Accuri C6 or CytoFLEX (Beckman Coulter) and sorted on a BD FACS AriaIII using FACSDiva software. All analyses and figures were done with FlowJo. All histograms were plotted with modal normalization.

Preparation of RNA-seq samples and alignment

For RNA-seq library preperation, cells were collected with Tri-Reagent (Sigma-Aldrich). Total RNA was extracted and poly-A selection was performed using Dynabeads mRNA DIRECT Purification Kit (Invitrogen) as described previously [49]. The mRNA samples were subjected to DNase I treatment and 3' dephosphorylation using FastAP Thermosensitive Alkaline Phosphatase (Thermo Scientific) and T4 polynucleotide kinase (New England Biolabs) followed by 3' adaptor ligation using T4 ligase (New England Biolabs). The ligated products were used for reverse transcription with SSIII (Invitrogen) for first-strand cDNA synthesis. The cDNA products were 3'-ligated with a second adaptor using T4 ligase and amplified for 8 cycles in a PCR for final library products of 200–300 bp. Raw sequences were first trimmed at their 3' end, removing the Illumina adapter and poly(A) tail. Alignment was performed using Bowtie 1[50] (allowing up to two mismatches) and reads were aligned to the human (hg19). Reads

aligned to ribosomal RNA were removed. Reads that were not aligned to the genome were then aligned to the transcriptome.

RNA labeling for SLAM-seq and analysis

For metabolic RNA labeling, 4sU (T4509, Sigma) was added at a final concentration of 200 µM to infected cells at 3h.p.i. Cells were collected with Tri-reagent at 2 and 3 h after adding the 4sU (corresponding to 5 and 6 h.p.i). RNA was extracted under reducing conditions and treated with iodoacetamide (A3221, Sigma) as previously described [18]. RNA-seq libraries were prepared and sequenced as described in 'Preparation of RNA-seq samples'.

Alignment of SLAM-seq reads was performed using STAR, with parameters that were previously described [51]. First, reads were aligned to a reference containing human rRNA and tRNA, and all reads that were successfully aligned were filtered out. The remaining reads were aligned to a reference of the human (hg19) and the TB40 (EF999921). In one analysis, the virus was analyzed as one transcript, and in a second analysis, all viral genes were analyzed. Output.bam files from STAR were used as input for the GRAND-SLAM analysis [52] with default parameters and with trimming of 5 nucleotides in the 5' and 3'ends of each read. Each one of the runs also included an unlabeled sample (no 4sU) that was used for estimating the linear model of the background mutations. The estimated ratio of newly synthesized out of total molecules for each viral and host genes were used for further analysis.

3D immunofluorescence viral DNA FISH

Differentiated monocytes (THP1 and CD14+) were seeded on 22X22 coverslips in a 6-well plate. Suspension monocytes were concentrated to 1M cells/150µl and seeded on 22X22 coverslips for 1 hour, followed by centrifuging for 10 min in 800g to deposit suspension cells onto the coverslips. FISH was done as previously described [53]. Cells were washed twice with PBS and fixed in 4% paraformaldehyde in PBS for 10 minutes. Then, cells were permeabilized in 0.5% triton/PBS for 15 minutes and rinsed in PBS. Samples were incubated in 20% glycerol/PBS at 4°C overnight and frozen five times in liquid nitrogen. Cells were washed three times in 0.05% triton/PBS, rinsed with PBS followed and with DDW. Cells were then incubated in 0.1M HCL for 15 minutes and then with 0.002% pepsin (Sigma, P6887)/0.01M HCl at 37°C for 90 seconds for monocytes or 75 seconds for macrophages, followed by inactivation in 50mM Mgcl2/PBS. Cells were then fixed in 1% paraformaldehyde/PBS for 1 minute and washed with PBS and with 2X SSC (Promega, V4261), followed by Incubation in 50%formamide/2X SSC (pH7-7.5) for 1 hour.

Probe was labeled according to the manufacturer instructions with TB40 SV40-GFP BAC DNA (Nick Translation Mix, Roche, 11745808910 and Tetramethyl-Rhodamine-5-dUTP, Roche 11534378910) and prepared for hybridization by combining 0.5mg of each labeled probe and 5mg cot-1 (Invitrogen, 15279-011) in 4.5µl deionized formamide (Sigma, F9037) and 4.5µl 4XSSC/20% dextran sulfate.
Following denaturation at 76°C, hybridization was performed at 37°C for 3 days. After hybridization, the coverslips were washed in 50% formamide/2X SSC (pH 7-7.5) at 37°C, in 0.5XSSC at 60°C and in 4XSSC/0.2%. Coverslips were mounted on slides with Prolong gold (Invitrogen, P36930) containing DAPI.

Immunofluorescence

For HCMV replication compartment detection, cells were plated on ibidi slides, fixed in 4% paraformaldehyde for 15 min, washed in PBS, permeabilized with 0.1% Triton X-100 in PBS for 10 min and then blocked with 10% goat serum in PBS for 30 min. Immunostaining was performed for the detection of mouse anti-UL44 (CA006-100, Virusys) with 2% goat serum. Cells were washed 3 times with PBS and labeled with goat anti-mouse–Alexa Fluor 647 (Thermo Fisher) secondary antibody and DAPI (4',6-diamidino-2-phenylindole) for 1 hour at room temperature.
Detection of the HCMV tegument protein (pp150, UL32) in the cytosol was performed by infecting the cells with the TB40-UL32-EGFP [30] for one hour, followed by three PBS washes and 15 minutes of fixation with 4% paraformaldehyde. Samples were mounted with DAPI for nuclear staining and Phalloidin to define cell borders.

Microscopy and Image Analysis

DNA-FISH and HCMV capsid images were taken using Leica TCS SP8 STED. DNA-FISH images were analyzed using Imaris10 software. HCMV capsid images were analyzed and quantified using ImagJ StarDist [54] and assigned to their corresponding cell ROIs. Images of HCMV replication compartment and bright field images were acquired on an AxioObserver Z1 wide-field microscope and analyzed using ImageJ.

Cell Surface Staining

Cells were washed three times with PBS and blocked for 15 min in 2% human serum. After blocking, cell staining was done using the following conjugated antibodies and their IgG controls: Allophycocyanin (APC)-conjugated mouse IgG2a anti-human Neuropilin-2 (R&D systems, catalog no.

FAB22151A) with allophycocyanin (APC)-conjugated mouse IgG2a control (R&D systems, catalog no. IC003A). Phycoerythrin (PE)-conjugated Mouse IgG2a anti-human PDGFRα (BD, catalog no. 556002) with phycoerythrin (PE)-conjugated Mouse IgG2a control (BD, catalog no. 555574). Alexa fluor 647 conjugated Mouse IgG1 anti-human CD61 (ITGB3) (BLG, catalog no. 336407) and Alexa fluor 647 conjugated Mouse IgG1 control (BLG, catalog no. 400130). FITC-conjugated Mouse IgG1 anti-human CD29 (ITGB1) (Santa cruz catalog no. *MEM-101A*) and FITC-conjugated Mouse IgG1 control (Santa Cruz, catalog no. sc-2339). Antibody incubation was done for 30 minutes at a 1:200 dilution. After staining, cells were washed twice with PBS and analyzed by flow cytometry.

Plasmids construction and lentiviral transduction

PDGFRα was cloned into pLex_TRC206 plasmid (Straussman et al., 2012) under EF-1α promoter and blasticidin selection. PDGFRα was amplified from cDNA and cloned into pLex by FastCloning[55].

For CRISPR knockout plasmids of NRP2, ITGB3 and ITGB1, we express two gRNAs in the LentiCRISPRv2 plasmid using restriction-free cloning to create a new plasmid called LentiCRISPRv2-2guide as previously described[56] (Table S4).

To generate an inducible expression plasmids of ITGB3 and ITGAV, genes were ordered from TWIST and were cloned into pLVX-Puro-TetONE-SARS-CoV-2-nsp1-2XStrep (kind gift from N. Krogan, UCSF) in place of the SARS-CoV-2-nsp1-2XStrep cassette using linearization with BamHI and EcoRI (neb). The genes were amplified with primers containing flanking regions homologous to the vector (Supplementary Table 4). The amplified PCR fragments were cleaned using a gel extraction kit (QIAGEN) according to the manufacturer's protocol and were cloned into the vectors using a Gibson assembly reaction (neb).

Lentiviral particles were generated by cotransfection of the expression constructs and second-generation packaging plasmids (psPAX2, Addgene, catalog no. 12260 and pMD2.G, Addgene, catalog no. 12259), using jetPEI DNA transfection reagent (Polyplus transfection) into 293T cells, according to the manufacturer's instructions. At 60 h post-transfection, supernatants were collected and filtered through a 0.45-µm polyvinylidene difluoride filter (Millex). THP1 cells were transduced with lentiviral particles by spinfection (800*g*, 1 h) and then selected with blasticidin (10 µg/ ml) for 5 days or puromycin (1.75 µg/ml) for 4 days. Blasticidin and puromycin were removed and cells were recovered for at least two days before subsequent differentiation.

Quantitative real-time PCR analysis

Total RNA was extracted using Direct-zol RNA Miniprep Kit (Zymo Research) following the manufacturer's instructions. cDNA was prepared using qScript FLEX cDNA Synthesis Kit (Quanta Biosciences) following the manufacturer's instructions. Real-time PCR was performed using SYBR Green PCR master-mix (ABI) on the QuantStudio 12K Flex (ABI). Amplification of NRP2 and ITGB3 was normalized to the host gene ANAX5 (primer detailed in table S4).

Total DNA was extracted using QIAamp DNA Blood kit (Qiagen) according to the manufacturer's instructions. Amplification of the viral gene UL44 was normalized to the host gene B2M (primer detailed in table S4).

Table S4 *primers list*

Primer number	sequence	Forward / reverse	Description
1	tcgtgagggatccaccATGGGGACTTCCCATCCGG	Forward	Amplification of PDGFRα from cDNA for FastCloning
2	cttaacgcgtctcgagTTACAGGAAGCTGTCTTCCAC	Reverse	
3	AGACAGCTTCCTGTAActcgagacgcgttaagtcga	Forward	Amplification of the pLex plasmid for PDGFRα FastCloning
4	CCGGATGGGAAGTCCCggtggatccctcacgacac	Reverse	
5	CACAACCatggccaagcctttg	Forward	Amplification of blasticidin from the pLEX plasmid for Gibson assembly to generate plvx-PDGFRα
6	gacgcttagccctcccacacataaccag	Reverse	

7	ggagggctaagcgtcgacaatcaacctct	Forward	Amplification of the plvx plasmid for Gibson assembly to generate plvx-PDGFRα
8	ttggccatGGTTGTGGCCATATTATCATCG	Reverse	
9	tacatcttgtggaaaggacgaaacaccgCGTTTGAATTCCAAAGATGCgttttagagctagaaatagcaagttaaaataaggc	Forward	2sg-NRP2 for NRP2 knockout
10	cttgctatttctagctctaaaacGGTTACCCCCAGGACTACCCgggaaagagtggtctcatacagaacttataag	Reverse	
11	tacatcttgtggaaaggacgaaacaccgGCAGGAGCTCACACCTCGCGgttttagagctagaaatagcaagttaaaataaggc	Forward	2sg-ITGB3 for ITGB3 knockout
12	cttgctatttctagctctaaaacCGCGTGGTACAGATGTTGGGgggaaagagtggtctcatacagaacttataag	Reverse	
13	tacatcttgtggaaaggacgaaacaccgGTGGAGAATGTATACAAGCAgttttagagctagaaatagcaagttaaaataaggc	Forward	2sg-ITGB1 for ITGB1 knockout
14	cttgctatttctagctctaaaacAATTGTGGGTGGTGCACAAAgggaaagagtggtctcatacagaacttataag	Reverse	
15	AATGGACTATCATATGCTTACCGTAACTTGAAAGTATTTCG	Forward	First PCR amplification for CRISPR screen
16	TGTGGGCGATGTGCGCTCTG	Reverse	
17	AATGATACGGCGACCACCGAGATCTACACTCTTTCCCTACACGACGCTCTTCCGATCTttcttgtggaaaggacgaaacacc	Forward	Second PCR amplification for CRISPR screen

18	CAAGCAGAAGACGGCATACGAG ATAAGTAGAG GTGACTGGAGTTCAGACGTGTG CTCTTCCGATCTgtgccactttttcaag ttgataac	Reverse	
19	AGTCTGGTCCTGCTTCACCT	Forward	ANAX5 for real-time PCR
20	CAAGCCTTTCATAGCCTTCC	Reverse	
21	CTGTGGGTCATCCGTGAGGAC	Forward	NRP2 for real-time PCR
22	ATGGGTTCCATGCAGTTCTCCAG	Reverse	
23	ACCAGTAACCTGCGGATTGG	Forward	ITGB3 for real-time PCR
24	TCCGTGACACACTCTGCTTC	Reverse	
25	TGCTGTCTCCATGTTTGATGTATCT	Forward	B2M for real-time PCR
26	TCTCTGCTCCCCACCTCTAAGT	Reverse	
27	AGCAAGGACCTGACCAAGTT	Forward	UL44 for real-time PCR
28	GCCGAGCTGAACTCCATATT	Reverse	
31	AATTCACCATGCGAGCGCGGC	Forward	For ITGB3 amplification to generate inducible TetOn- ITGB3

32	CTGGATCCttaAGTGCCCCGGTACGTGA	Reverse	
35	ccctcgtaaagaattATGCTCCTAGGCACCCTCC	Forward	For ITGAV amplification to generate inducible TetOn- ITGAV
36	gaggtggtctggatcTTAAGTTTCTGAGTTTCCTTCACCATTTTCATGAG	Reverse	

CRISPR screen (transduction, selection, FACS sorting, DNA extraction and data analysis)

THP1 cells that overexpress PDGFRα were transduced with the GeCKO V2 library (addgene, library A) lentiviral particles using spinfection (800 g for 1 h) at low MOI= 0.3 in 6-well plates. Two days later, transduced cells were selected with 1.75 ug/ml puromycin for 4 days and were recovered from the selection for two days. Cells were then infected with HCMV-GFP at MOI = 5 and after two days were sorted to GFP-bright and GFP-dim cells from which DNA was extracted using QIAamp DNA blood mini kit (QIAGEN).

gRNAs were PCR amplified by a two-step PCR. The first PCR amplifies the target region which is used as a template for the second PCR (Table S4). In each PCR reaction, 1µg template for the first PCR and 40ng for the second PCR was amplified using NEBNext master mix (NEB, M0541) and cleaned using SPRI beads (BECKMAN COULTER), after the first PCR with 2-sided 0.5X and 1.8X cleanup, and after the second PCR with 0.9X.

MAGeCK v0.5.6 was used to count gRNA from FASTQ files and to analyze the selection effect of genes based on the change in gRNA distribution, using the robust rank aggregation (RRA) algorithm with normalization to total reads. Directed FDR and RRA scores for genes were calculated by setting the sign of the enrichment or depletion MAGeCK FDR and RRA scores respectively according to the sign of the gene fold change.

The entire CRISPR screen was done twice, with two separate infections for each screen.

Differential expression and enrichment analysis

Differential expression analysis on RNA-seq data was performed with DESeq2 (v.1.22.2) using default parameters, with the number of reads in each of the samples as an input.

The log_2(fold change) values from the DE on the RNA-seq and the transformed score from the MAGeCK output of the CRISPR screen (log10 on the MAGeCK score, and multiplication of -1 on the negative log fold change values) were used for enrichment analysis using GSEA (v.4.1). For the analysis, only genes with a minimum of ten reads were included.

Oxidative phosphorylation measurement and inhibition

For Oxidative phosphorylation rate measurement, 100nM TMRM (Tetramethylrhodamine) was added to the cells for 30 minutes at 37°C, followed by PBS washing before FACS analysis.
For Oxidative phosphorylation inhibition, CCCP (sigma) was added to the cells at a final concentration of 5uM 1 h before infection.

PI staining for cell cycle analysis and cell viability

For cell cycle measurement, cells were washed three times with PBS, followed by fixation in 70% cold EtOH overnight at -20°C. Cells were washed with PBS twice and treated with RNaseA 0.2mg/ml for 30 minutes at room temperature. 0.01mg/ml PI (sigma) was added before FACS analysis. For measuring cell viability, cells were washed in PBS and treated with 0.01mg/ml PI for 20 min at room temperature before analyzing the cells by flow cytometry.

Acknowledgments

We thank Dr. Orly Laufman, Prof. Yossef Shaul and the members of the Stern-Ginossar lab for the critical reading of the manuscript. We thank Dr. Dor Simkin and Dr. Avner Leshem for the blood extraction. We thank the Weizmann flow cytometry and microscopy unit for technical assistance. This study was supported by a European Research Council consolidator grant (CoG-2019-864012) and an Israel Science Foundation grant to N.S.-G. (2507/23).

Author contributions

Y.K., N.S.-G. and M.S. conceived and designed the project. Y. K., T.A., A.W. and M.S. performed the experiments. T.F. helped analyze the HCMV particle images. Y.F. offered valuable guidance throughout the research. Y.K., A.N., N.S-G and M.S. analyzed and interpreted the data. Y.K., N.S.-G. and M.S. wrote the manuscript with input from all the authors.

References

1. Hahn, G., Jores, R. & Mocarski, E. S. Cytomegalovirus remains latent in a common precursor of dendritic and myeloid cells. *Proc. Natl. Acad. Sci. U. S. A.* **95**, 3937–3942 (1998).
2. Kondo, K., Kaneshima, H. & Mocarski, E. S. Human cytomegalovirus latent infection of granulocyte-macrophage progenitors. *Proc. Natl. Acad. Sci. U. S. A.* **91**, 11879–11883 (1994).
3. Taylor-Wiedeman, J., Sissons, J. G., Borysiewicz, L. K. & Sinclair, J. H. Monocytes are a major site of persistence of human cytomegalovirus in peripheral blood mononuclear cells. *J. Gen. Virol.* **72 (Pt 9)**, 2059–2064 (1991).
4. Cheng, S. *et al.* Transcriptome-wide characterization of human cytomegalovirus in natural infection and experimental latency. *Proc. Natl. Acad. Sci. U. S. A.* **114**, E10586–E10595 (2017).
5. Sinzger, C., Plachter, B., Grefte, A., The, T. H. & Jahn, G. Tissue macrophages are infected by human cytomegalovirus in vivo. *J. Infect. Dis.* **173**, 240–245 (1996).
6. Ibanez, C. E., Schrier, R., Ghazal, P., Wiley, C. & Nelson, J. A. Human cytomegalovirus productively infects primary differentiated macrophages. *J. Virol.* **65**, 6581–6588 (1991).
7. Reeves, M. B., Lehner, P. J., Sissons, J. G. P. & Sinclair, J. H. An in vitro model for the regulation of human cytomegalovirus latency and reactivation in dendritic cells by chromatin remodelling. *J. Gen. Virol.* **86**, 2949–2954 (2005).
8. Taylor-Wiedeman, J., Sissons, P. & Sinclair, J. Induction of endogenous human cytomegalovirus gene expression after differentiation of monocytes from healthy carriers. *J. Virol.* **68**, 1597–1604 (1994).
9. Schwartz, M. *et al.* Molecular characterization of human cytomegalovirus infection with single-cell transcriptomics. *Nat Microbiol* (2023) doi:10.1038/s41564-023-01325-x.
10. Elder, E. & Sinclair, J. HCMV latency: what regulates the regulators? *Medical Microbiology and Immunology* vol. 208 431–438 Preprint at https://doi.org/10.1007/s00430-019-00581-1 (2019).
11. Champion, A. *et al.* MORC3 represses the HCMV major immediate early promoter in myeloid cells in the absence of PML nuclear bodies. *J. Med. Virol.* **95**, e29227 (2023).
12. Goodrum, F. Human Cytomegalovirus Latency: Approaching the Gordian Knot. *Annual Review of Virology* vol. 3 333–357 Preprint at https://doi.org/10.1146/annurev-virology-110615-042422 (2016).
13. Hussein, H. A. M. *et al.* Beyond RGD: virus interactions with integrins. *Arch. Virol.* **160**, 2669–2681 (2015).

14. Feire, A. L., Koss, H. & Compton, T. Cellular integrins function as entry receptors for human cytomegalovirus via a highly conserved disintegrin-like domain. *Proc. Natl. Acad. Sci. U. S. A.* **101**, 15470–15475 (2004).

15. O'Connor, C. M. & Murphy, E. A. A myeloid progenitor cell line capable of supporting human cytomegalovirus latency and reactivation, resulting in infectious progeny. *J. Virol.* **86**, 9854–9865 (2012).

16. Terhune, S. S., Schröer, J. & Shenk, T. RNAs are packaged into human cytomegalovirus virions in proportion to their intracellular concentration. *J. Virol.* **78**, 10390–10398 (2004).

17. Rozman, B. *et al.* Temporal dynamics of HCMV gene expression in lytic and latent infections. *Cell Rep.* **39**, 110653 (2022).

18. Herzog, V. A. *et al.* Thiol-linked alkylation of RNA to assess expression dynamics. *Nat. Methods* **14**, 1198–1204 (2017).

19. Gažová, I. *et al.* The Transcriptional Network That Controls Growth Arrest and Macrophage Differentiation in the Human Myeloid Leukemia Cell Line THP-1. *Front Cell Dev Biol* **8**, 498 (2020).

20. Traore, K. *et al.* Signal transduction of phorbol 12-myristate 13-acetate (PMA)-induced growth inhibition of human monocytic leukemia THP-1 cells is reactive oxygen dependent. *Leuk. Res.* **29**, 863–879 (2005).

21. Salvant, B. S., Fortunato, E. A. & Spector, D. H. Cell cycle dysregulation by human cytomegalovirus: influence of the cell cycle phase at the time of infection and effects on cyclin transcription. *J. Virol.* **72**, 3729–3741 (1998).

22. Fortunato, E. A., Sanchez, V., Yen, J. Y. & Spector, D. H. Infection of cells with human cytomegalovirus during S phase results in a blockade to immediate-early gene expression that can be overcome by inhibition of the proteasome. *J. Virol.* **76**, 5369–5379 (2002).

23. Goodrum, F. The complex biology of human cytomegalovirus latency. *Adv. Virus Res.* **112**, 31–85 (2022).

24. Dooley, A. L. & O'Connor, C. M. Regulation of the MIE Locus During HCMV Latency and Reactivation. *Pathogens* **9**, (2020).

25. Tong, J. K., Hassig, C. A., Schnitzler, G. R., Kingston, R. E. & Schreiber, S. L. Chromatin deacetylation by an ATP-dependent nucleosome remodelling complex. *Nature* **395**, 917–921 (1998).

26. Poole, E. & Sinclair, J. Latency-associated upregulation of SERBP1 is important for the recruitment of transcriptional repressors to the viral major immediate early promoter of human cytomegalovirus during latent carriage. *Front. Microbiol.* **13**, 999290 (2022).

27. Saffert, R. T. & Kalejta, R. F. Human cytomegalovirus gene expression is silenced by Daxx-mediated intrinsic immune defense in model latent infections established in vitro. *J. Virol.* **81**, 9109–9120 (2007).

28. Nguyen, C. C. & Kamil, J. P. Pathogen at the Gates: Human Cytomegalovirus Entry and Cell Tropism. *Viruses* **10**, (2018).

29. Martinez-Martin, N. *et al.* An Unbiased Screen for Human Cytomegalovirus Identifies Neuropilin-2 as a Central Viral Receptor. *Cell* **174**, 1158–1171.e19 (2018).

30. Sampaio, K. L., Cavignac, Y., Stierhof, Y.-D. & Sinzger, C. Human cytomegalovirus labeled with green fluorescent protein for live analysis of intracellular particle movements. *J. Virol.* **79**, 2754–2767 (2005).

31. Soroceanu, L., Akhavan, A. & Cobbs, C. S. Platelet-derived growth factor-alpha receptor activation is required for human cytomegalovirus infection. *Nature* **455**, 391–395 (2008).

32. Wang, X., Huang, D. Y., Huong, S.-M. & Huang, E.-S. Integrin alphavbeta3 is a coreceptor for human cytomegalovirus. *Nat. Med.* **11**, 515–521 (2005).

33. Maidji, E., Genbacev, O., Chang, H.-T. & Pereira, L. Developmental regulation of human cytomegalovirus receptors in cytotrophoblasts correlates with distinct replication sites in the placenta. *J. Virol.* **81**, 4701–4712 (2007).

34. Pellagatti, A. *et al.* Impact of spliceosome mutations on RNA splicing in myelodysplasia: dysregulated genes/pathways and clinical associations. *Blood* **132**, 1225–1240 (2018).

35. Johnsen, H. E. *et al.* Selective loss of progenitor subsets following clinical CD34+ cell enrichment by magnetic field, magnetic beads or chromatography separation. *Bone Marrow Transplant.* **24**, 1329–1336 (1999).

36. Sanjana, N. E., Shalem, O. & Zhang, F. Improved vectors and genome-wide libraries for CRISPR screening. *Nat. Methods* **11**, 783–784 (2014).

37. Li, W. *et al.* MAGeCK enables robust identification of essential genes from genome-scale CRISPR/Cas9 knockout screens. *Genome Biol.* **15**, 554 (2014).

38. Compton, T., Nowlin, D. M. & Cooper, N. R. Initiation of human cytomegalovirus infection requires initial interaction with cell surface heparan sulfate. *Virology* **193**, 834–841 (1993).

39. Shnayder, M. *et al.* Defining the Transcriptional Landscape during Cytomegalovirus Latency with Single-Cell RNA Sequencing. *MBio* **9**, (2018).

40. Rauwel, B. *et al.* Release of human cytomegalovirus from latency by a KAP1/TRIM28 phosphorylation

switch. *Elife* **4**, (2015).

41. Poole, E. *et al.* A BMPR2/YY1 Signaling Axis Is Required for Human Cytomegalovirus Latency in Undifferentiated Myeloid Cells. *MBio* **12**, e0022721 (2021).
42. Poole, E. *et al.* The myeloid transcription factor GATA-2 regulates the viral UL144 gene during human cytomegalovirus latency in an isolate-specific manner. *J. Virol.* **87**, 4261–4271 (2013).
43. Kim, J. H., Collins-McMillen, D., Caposio, P. & Yurochko, A. D. Viral binding-induced signaling drives a unique and extended intracellular trafficking pattern during infection of primary monocytes. *Proc. Natl. Acad. Sci. U. S. A.* **113**, 8819–8824 (2016).
44. Feire, A. L., Roy, R. M., Manley, K. & Compton, T. The glycoprotein B disintegrin-like domain binds beta 1 integrin to mediate cytomegalovirus entry. *J. Virol.* **84**, 10026–10037 (2010).
45. Bogdanow, B. *et al.* Human cytomegalovirus tegument protein pp150 acts as a cyclin A2-CDK-dependent sensor of the host cell cycle and differentiation state. *Proc. Natl. Acad. Sci. U. S. A.* **110**, 17510–17515 (2013).
46. Munger, J., Bajad, S. U., Coller, H. A., Shenk, T. & Rabinowitz, J. D. Dynamics of the cellular metabolome during human cytomegalovirus infection. *PLoS Pathog.* **2**, e132 (2006).
47. Combs, J. A. *et al.* Human Cytomegalovirus Alters Host Cell Mitochondrial Function during Acute Infection. *J. Virol.* **94**, (2020).
48. Betsinger, C. N. *et al.* The human cytomegalovirus protein pUL13 targets mitochondrial cristae architecture to increase cellular respiration during infection. *Proc. Natl. Acad. Sci. U. S. A.* **118**, e2101675118 (2021).
49. Shishkin, A. A. *et al.* Simultaneous generation of many RNA-seq libraries in a single reaction. *Nat. Methods* **12**, 323–325 (2015).
50. Langmead, B., Trapnell, C., Pop, M. & Salzberg, S. L. Ultrafast and memory-efficient alignment of short DNA sequences to the human genome. *Genome Biol.* **10**, R25 (2009).
51. Fisher, T. *et al.* Parsing the role of NSP1 in SARS-CoV-2 infection. *Cell Rep.* **39**, 110954 (2022).
52. Jürges, C., Dölken, L. & Erhard, F. Dissecting newly transcribed and old RNA using GRAND-SLAM. *Bioinformatics* **34**, i218–i226 (2018).
53. Skowronska-Krawczyk, D. *et al.* Required enhancer-matrin-3 network interactions for a homeodomain transcription program. *Nature* **514**, 257–261 (2014).

54. Schmidt, U., Weigert, M., Broaddus, C. & Myers, G. Cell detection with star-convex polygons. *arXiv [cs.CV]* (2018).

55. Li, C. *et al.* FastCloning: a highly simplified, purification-free, sequence- and ligation-independent PCR cloning method. *BMC Biotechnol.* **11**, 92 (2011).

56. Finkel, Y. *et al.* A virally encoded high-resolution screen of cytomegalovirus dependencies. *Nature* **630**, 712–719 (2024).

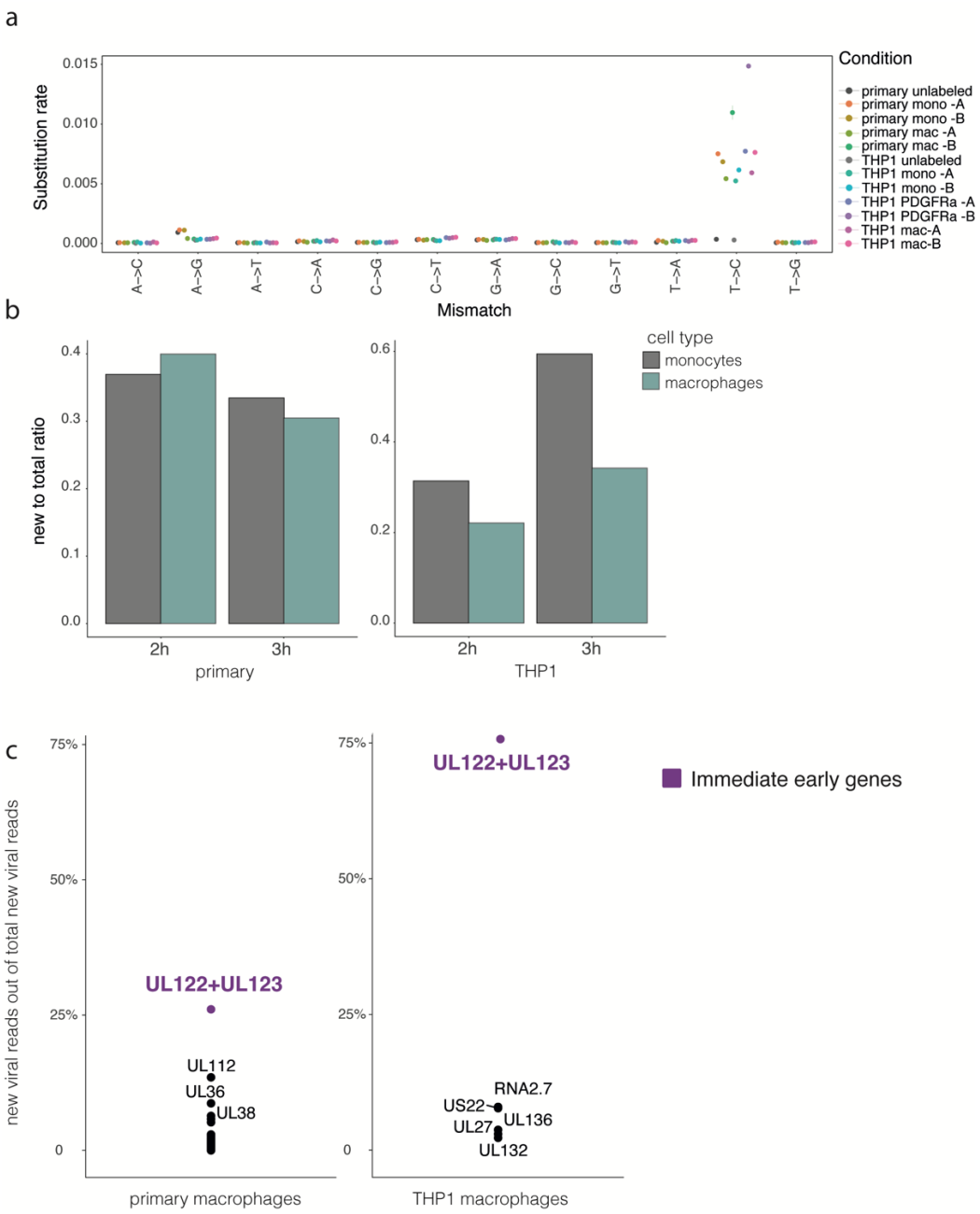

Fig. S1. (a). Rates of nucleotide substitutions demonstrate efficient conversion rates in 4sU-treated samples compared to unlabeled cells (no 4sU, gray dots). Mono, monocytes; mac, macrophages. (b). Proportion of new-to-total RNA of cellular transcripts in infected primary and THP1 monocytes and macrophages. Infected cells were labeled with 4sU at 3 h.p.i. and collected for RNAseq after two (left bars) or three (adjacent right bars) hours post labeling. (c). Percentage of new viral gene reads out of total new viral reads in infected primary and THP1 macrophages at three hours post labeling (6 h.p.i).

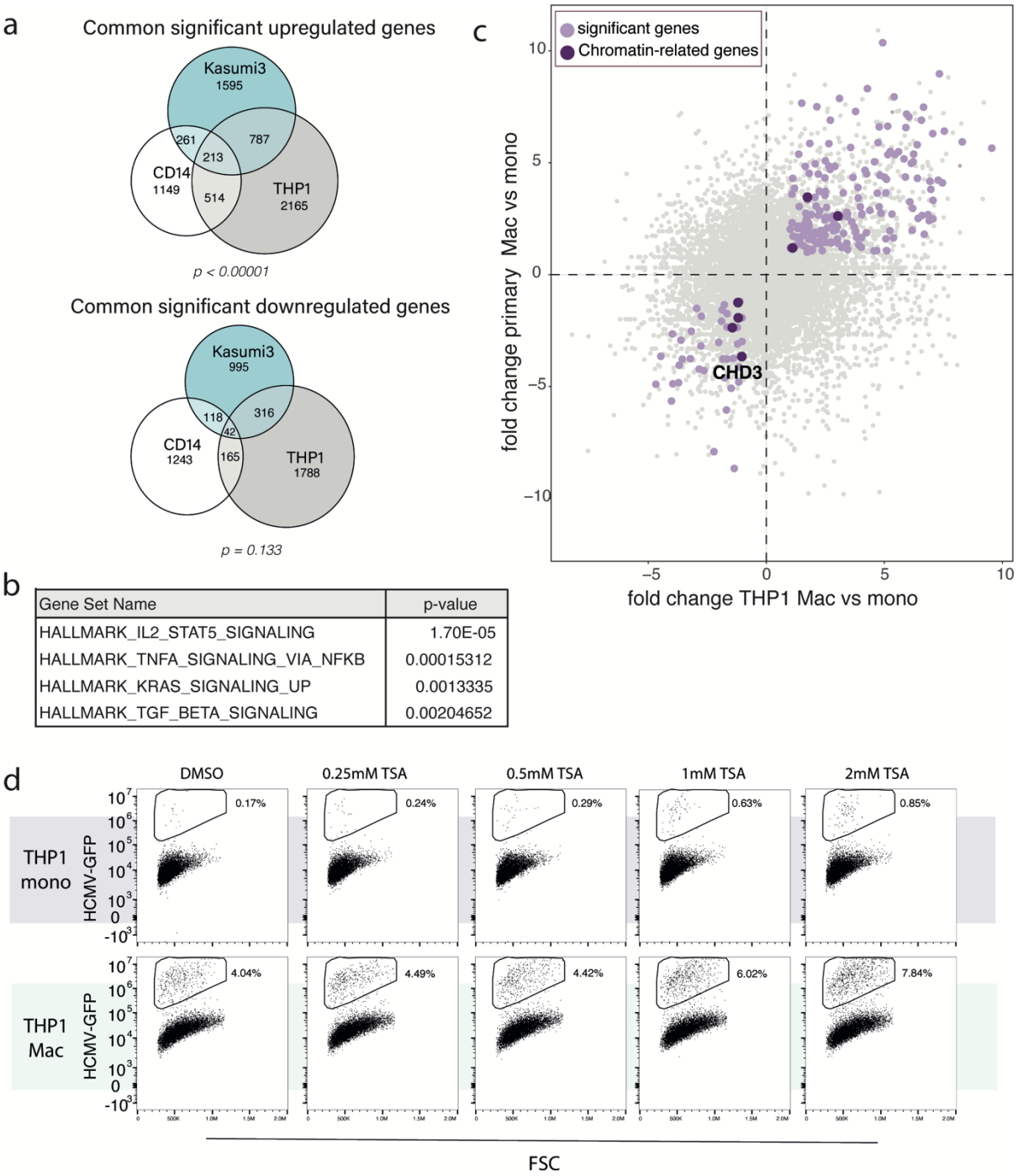

Gene Set Name	p-value
HALLMARK_IL2_STAT5_SIGNALING	1.70E-05
HALLMARK_TNFA_SIGNALING_VIA_NFKB	0.00015312
HALLMARK_KRAS_SIGNALING_UP	0.0013335
HALLMARK_TGF_BETA_SIGNALING	0.00204652

Fig. S2. (a). Venn diagram summarizing the amount of significant upregulated and downregulated genes in all three cell types. Statistics on the common upregulated and downregulated genes were performed using hypergeometric test. (b). Hallmark pathway enrichment analysis shows four significantly enriched pathways in the 213 common significant upregulated genes. Analysis was performed using a hypergeometric test.

(c). Scatterplot of the fold change (FC) from RNA-seq data between primary monocytes and macrophages, relative to the fold change of THP1 monocytes and macrophages. Purple dots represent significantly upregulated genes in all three cell types. Dark purple dots represent chromatin-related genes that are significantly changing

upon differentiation in all three cell types (p = 0.885 for the downregulated and p = 0.999 for the upregulated genes using a hypergeometric test). (d). Flow cytometry analysis of infected THP1 monocytes and macrophages, treated with TSA or DMSO as control at 5 h.p.i. Analysis was performed at 3 d.p.i. The gate marks the productive, GFP-bright cell population.

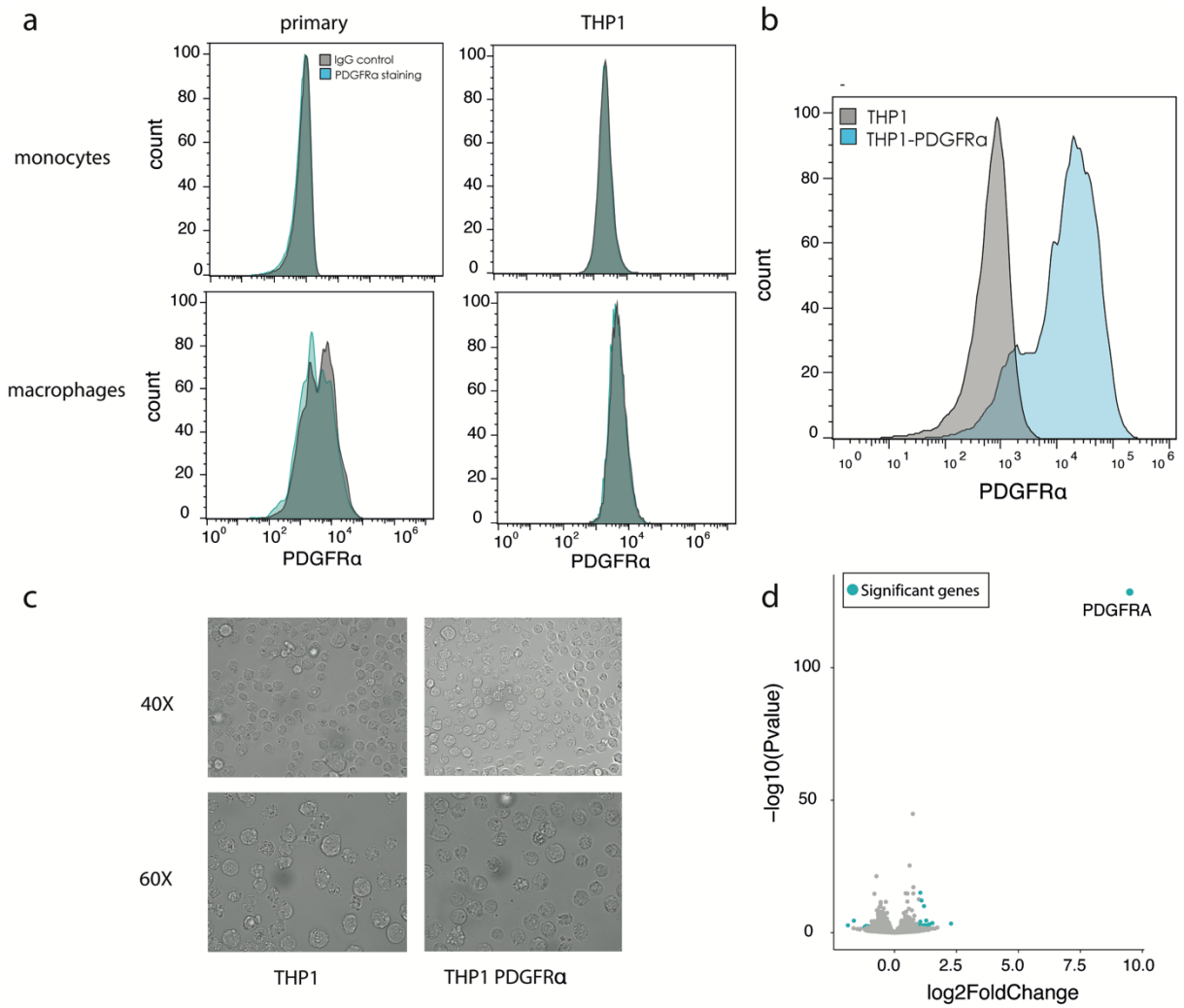

Fig. S4. (a). Flow cytometry analysis of cell surface staining of PDGFRα versus IgG control in primary and THP1 monocytes and macrophages. (b). Flow cytometry analysis of cell surface staining of PDGFRα of THP1 and THP1-PDGFRα monocytes. (c). Light microscopy of THP1 and THP1-PDGFRα monocytes. (d). Differential expression analysis of RNA-seq from THP1 and THP1-PDGFRα monocytes. Blue dots mark significant differentially expressed genes ($p < 0.05$, FC > 1).

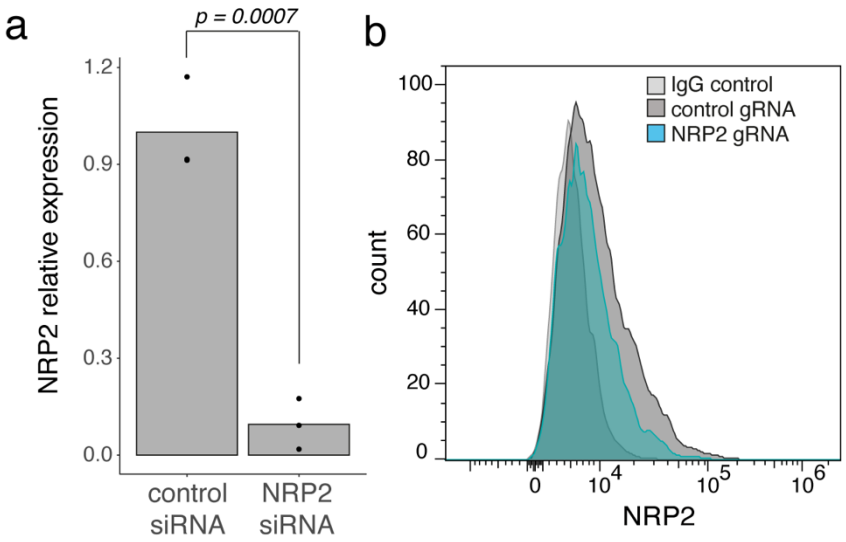

Fig. S5. (a). Relative expression level of NRP2, measured by real-time PCR in THP1 macrophages treated with NRP2 siRNA compared to control siRNA at 0 h.p.i. (b) Cell surface staining with NRP2 or IgG control of THP1 macrophages treated with CRISPR knockout against NRP2 or control. Cells were analyzed by Flow cytometry.

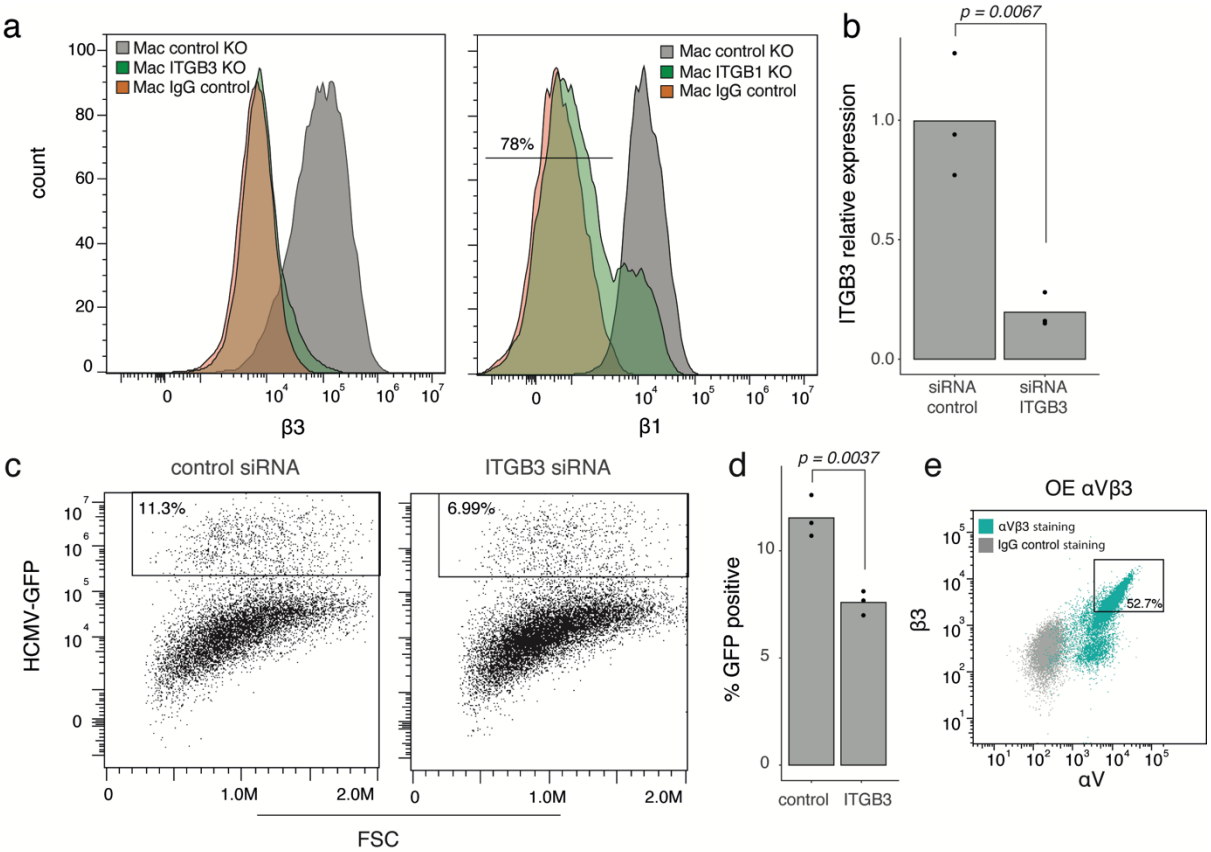

Fig. S6. (a). Cell surface staining of THP1 macrophages with a CRISPR knockout of β3 (left), β1 (right), or both versus control knockout. Cells were analyzed by Flow cytometry. (b). real-time PCR analysis of THP1 macrophages treated with siRNA against ITGB3 or control at 0 h.p.i.. (c). Flow cytometry analysis of THP1 macrophages, transfected with ITGB3 or control siRNAs and infected with HCMV–GFP. Cells were analyzed at 3 d.p.i. (d). Quantification of the FACS replicates of Fig. 5c. (e). Cell surface staining of THP1 overexpressing (OE) αVβ3 compared to IgG control. Cells were stained for both αV and β3 in the αVβ3 overexpressing cells. Double positive cells are gated in a box.

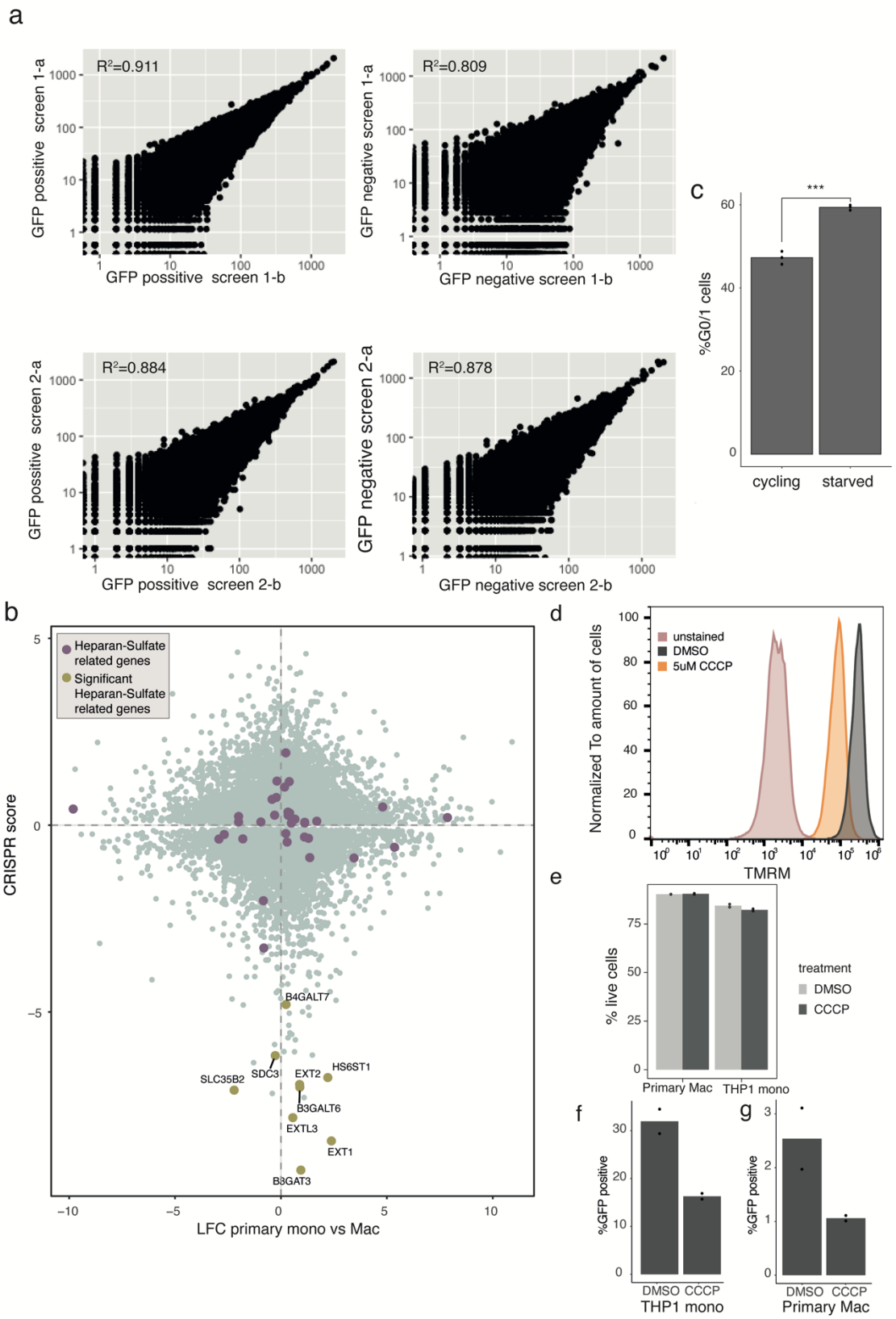

Fig. S7. *(*a). Correlation plot between biological replicates of the GFP-bright and GFP-dim sorted cells from the screens. (b). Scatter plot of MaGECK score of each gene versus log fold change (LFC) of expression in primary monocytes versus macrophages. Genes related to heparan-sulfate are marked in purple, and the significant

heparan-sulfate downregulated genes from the screen (FDR < 0.05, LFC > |1|) are marked in yellow and indicated by name. (c) Percentage of cells in G0/G1 phase. THP1 monocytes grown in 20% or 0.5% FBS (cycling and starved cells, respectively) were stained with PI. Cells were analyzed by flow cytometry and the cell cycle stage of the cells was determined using FlowJo software. (d). Oxidative phosphorylation measurement by TMRM staining of THP1 treated with 5µM CCCP or DMSO as a control for 1 hour. Cells were analyzed by flow cytometry. (e). Cell viability as measured by PI staining in THP1 monocytes and primary macrophages that were treated with 5µM CCCP or DMSO for 1 hour. Cells were analyzed using Flow Cytometry. (f). Quantification of the %GFP positive cells in the FACS replicates presented in Fig. 7e. (g). Quantification of the %GFP positive cells from the FACS replicates presented in Fig. 7g.